New Dimensions in Catalysis Research with Hard X-Ray Tomography

Srashtasrita Das[1], Reihaneh Pashminehazar[1], Shweta Sharma[1], Sebastian Weber[1,2], and Thomas L. Sheppard[1,2],*

The structure and function of solid catalysts are inseparably linked at length scales from nm to cm and beyond. Hard X-ray tomography offers unique potential for spatially-resolved characterization by combining flexible spatial resolution with a range of chemical contrasts. However, the full capabilities of hard X-ray tomography have not been widely explored in the catalysis community. This review highlights modern advances in hard X-ray tomography using synchrotron radiation. Case studies from model to technical scale illustrate the bright future of X-ray tomography in catalysis research.

1 Introduction

Catalysis drives the majority of chemical processes involved in production of essential chemicals, fuels, and commodities [1]. Furthermore, catalysis plays a vital role in promoting energy- and material-efficient chemical reactions, leading to a cleaner and more sustainable chemical industry [2, 3]. The transition of solid catalysts from laboratory scale into technical or industrial applications leads to a huge parameter space in terms of catalyst composition and structure. Structural features of solid catalysts cover length scales from sub-nm active catalytic sites, to nm-scale metal clusters or nanoparticles, to multiscale micro- (< 2 nm), meso- (2–50 nm), and macropore (> 50 nm) networks, all the way up to shaped solid catalyst bodies on the µm- to cm-scale [1, 4, 5]. Therefore, solid catalysts are typically complex in nature and may contain multiple components or hierarchical structural features, each of which are related to the catalytic function [6, 7].

Structural analysis at all length scales is crucial for a detailed understanding of catalyst structure-activity relationships [8, 9]. However, many catalyst characterization methods are performed in bulk and provide only averaged data. For example, catalyst porosity and surface area are often derived from gas sorption, e.g., with N_2 or Ar, and mercury intrusion [10, 11]. Such bulk porosimetry methods typically produce a single result representing average pore size or surface area but may have difficulty to probe bimodal or multimodal pore systems in hierarchically-porous materials. Complex properties, such as tortuosity, connectivity, or pore shape, are also generally out of reach using bulk analysis. As another example, while in situ or operando measurements are valuable for studying catalyst structure-function relations under working conditions, bulk characterization by spectroscopy or diffraction may fail to address the complexity of an active catalyst. Examples are X-ray absorption spectroscopy (XAS) or powder X-ray diffraction (XRD), two common methods for studying metal active sites and crystalline phase composition, respectively [12–14]. These measurement techniques can be employed by utilizing X-rays of different energy ranges. In catalysis research, these ranges are typically classified as soft (approx. < 2 keV), tender (approx. 2–5 keV), and hard (approx. > 5 keV) X-rays. However, this classification is not universal and may differ in other scientific fields. Using high energy or hard X-rays, methods such as XAS and XRD probe the average composition of a catalyst along the entire transmitted beam path. This leads to overlapping signals and reduced sensitivity to mixed oxidation states, mixed crystalline phases, or minor structural components of the solid catalyst. Distinguishing the catalyst surface from interior structure is similarly challenging in these circumstances.

[1]Srashtasrita Das, Dr. Reihaneh Pashminehazar, Shweta Sharma, Sebastian Weber, Dr. Thomas L. Sheppard
thomas.sheppard@kit.edu
Karlsruhe Institute of Technology, Institute for Chemical Technology and Polymer Chemistry, Engesserstraße 18, 76131 Karlsruhe, Germany.

[2]Sebastian Weber, Dr. Thomas L. Sheppard
Karlsruhe Institute of Technology, Institute of Catalysis Research and Technology, Hermann-von-Helmholtz Platz 1, 76344 Eggenstein-Leopoldshafen, Germany.

The situation becomes even more complex when considering dynamic spatial and chemical gradients, which may occur in the catalyst during reactor start-up and shutdown or during reaction [15].

To account for structural heterogeneity in solid catalysts across all relevant length scales, the concept of spatially resolved characterization is key [6, 8, 9, 16–19]. This involves highly localized characterization of specific regions of a catalyst sample, with sensitivity to the local structure or chemical composition. In this context, hard X-rays constitute a flexible and powerful probe for spatially-resolved catalyst characterization, due to their high penetration depth in solid matter and a range of sample interactions including absorption, diffraction, and fluorescence. Well-known methods such as XAS, XRD, and X-ray photoelectron spectroscopy (XPS) are now routinely applied for spatially-resolved catalyst characterization with bulk or surface sensitivity. A recent review by Mino et al. summarizes many spatially-resolved applications of X-rays, though this does not include all possible techniques and is not limited to catalysis [20].

A major application of hard X-rays which is less known among the catalysis community is hard X-ray microscopy and tomography [21–23]. These methods generate spatially-resolved images of the catalyst sample, allowing to distinguish local signals in 2D (microscopy, radiography) and 3D space (tomography). 2D X-ray microscopy or single projection imaging provides spatial information on the sample without any depth contrast, whereas a tomographic reconstruction is obtained using a projection series of 2D images at different rotational angles, which are then reconstructed to provide 3D spatial compositional or structural information. Hence, tomography can outperform surface- or bulk-sensitive measurements to provide a compositional view of the entire sample in 3D space. A crucial advantage of hard X-ray tomography over contemporary structural analysis methods is that it can noninvasively probe the sample interior without significant structural damage. As a result of these unique capabilities, X-ray tomography has already revolutionized the fields of diagnostic medicine and materials science since first practical demonstrations in the 1980s. Additionally, modern developments make X-ray tomography highly attractive for studying catalysts and other functional materials.

The growing potential of X-ray tomography in catalysis research is mainly driven by the development of synchrotron light sources. These large-scale research infrastructures offer extremely high-quality X-rays with high intensity, tunable energy, and broad experimental flexibility [13, 19, 22, 23]. Using hard X-rays produced at the synchrotron, it is now possible to perform tomographic studies:

– over a wide range of sample sizes, e.g., μm- to cm-scale, and with variable spatial resolution, e.g., nm- to μm-scale, to address hierarchically structured materials, or length scales ranging from single catalyst grains to small chemical reactors.

– with various chemical contrast modes, allowing to map, e.g., crystalline phase distributions with XRD tomography, metal distribution on catalyst supports with X-ray fluorescence (XRF) tomography, or metal oxidation state and coordination environment with XAS tomography in 3D space.

– using in situ or operando measurements, where the catalyst or reactor is in a chemically active state, allowing direct visualization of structural and chemical gradients linked to the physicochemical behavior of the catalyst.

An illustrative overview of a typical synchrotron experiment is shown in Fig. 1a, including a summary of several contrast modes for tomographic studies in Fig. 1b which have become significant in catalysis literature and are reviewed in the present work. Furthermore, Fig. 1c summarizes the parameter space which is relevant when considering or planning an X-ray tomography experiment. In general, the golden rule of tomographic measurements must be observed, meaning that from (maximum) spatial resolution, (maximum) sample size, and (minimum) scan duration, two out of these three parameters can be optimized in a given experiment, but typically not all three. Specific values are included as examples with specific case studies below. However, it should be noted that as hard X-ray tomography is a rapidly developing method, any numbers presented here regarding spatial resolution, sample size, and scan duration should not be regarded as hard limits. In fact, the methodology is highly flexible and dependent on the aims of the specific study, whether this is high throughput imaging, maximum spatial resolution, or time-resolved imaging.

Currently, a large proportion of synchrotron research in catalysis is based on academic or fundamental studies. However, synchrotrons also hold strong potential for joint projects at higher technology readiness level, based on cooperation between industry, academia, and synchrotron scientists. To foster the development of hard X-ray tomography for catalysis research with industrially relevant or technical applications, the missing ingredient is simply awareness of the benefits of synchrotron radiation within the broader catalysis community. The current review highlights concrete examples in which hard X-ray tomography has driven forward our understanding of heterogeneous catalysis, from model systems to technical scale. The strong focus here on tomography or 3D imaging emphasizes and exploits the excellent depth contrast available through use of hard X-rays, which is not taken advantage of in conventional 2D imaging. Three selected topic areas are used to demonstrate the broad characterization potential of hard X-ray tomography: 1) multiscale imaging, 2) chemical imaging, and 3) in situ/operando imaging. Previous reviews including tomography and catalysis have focused on general principles of X-ray microscopy [20], spatially resolved imaging with various probes [8, 18], in situ applications [9, 22], specific material classes such as zeolite catalysts [24], specific contrast modes like X-ray diffraction [25], and
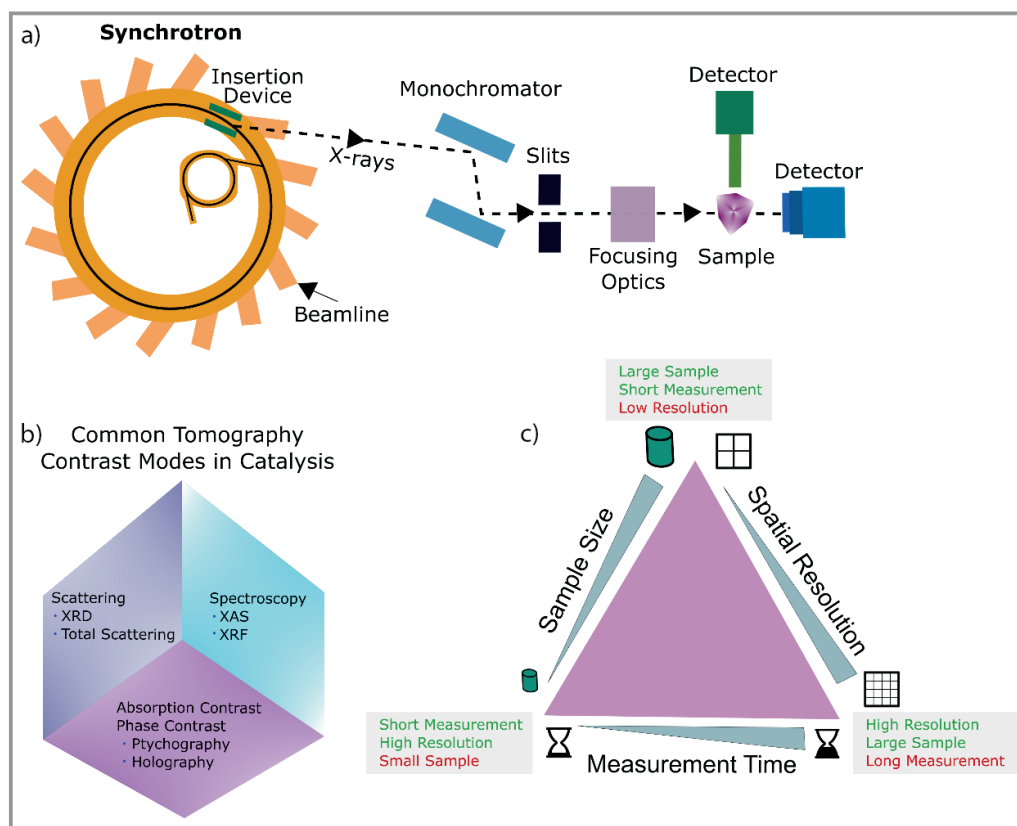
Figure 1. a) An illustrative overview of a synchrotron radiation facility showing a typical beamline facilitating sample characterization; b) different tomography modes available for sample characterization using hard X-rays for ex situ, in situ, and operando heterogeneous catalytic systems; c) the golden rule for tomographic studies using three important measurement parameters.

illustrated the surprising rate at which novel characterization tools are developed [19]. In this context, the current review focuses on specific catalyst case studies and covers the most notable modern developments of hard X-ray tomography. The aim is to stimulate the interest of catalysis researchers in industry, academia, and the synchrotron community, charting modern progress in this field, and highlighting the bright future of synchrotron X-ray tomography in catalysis research.

2 Hard X-Ray Tomography Bridging Different Length Scales in Heterogeneous Catalysis

Heterogeneous catalysis is a multiscale phenomenon by nature. Multiple length scales must be addressed during characterization to build a complete picture of catalyst structure and function. The major length scales of relevance to solid catalysts are illustrated in Fig. 2. For a typical catalytic process, it can be readily observed that length scales from the reactor (m) down to the active sites (sub-nm) must be covered. In fact, a range of 3D imaging methods are available to address these length scales. The tomograms illustrated in Fig. 2 are all acquired for the same Ni/Al$_2$O$_3$

catalyst material (labeled SPP2080-IMRC) [26], highlighting different tomography methods and length scales observable using hard X-ray, ion, and electron sources.

As illustrated in Fig. 2 and the attached scale bar, no single tomography method can analyze all possible length scales. On the contrary, a combination of complementary methods is essential. However, the choice of individual methods inevitably results in a trade-off between sample size, spatial resolution, and representativeness of the chosen sample (Fig. 1c). For example, this review focuses on hard X-ray tomography, offering a broad range of spatial resolutions between those of optical microscopy (several hundred nm) and electron microscopy (sub-nm). At lower resolution, e.g., 1–10 μm, hard X-ray microtomography is now relatively routine both using synchrotron X-rays and laboratory X-ray sources, and is applicable even to large samples, e.g., mm or cm. At higher resolution, modern X-ray nanotomography methods at the synchrotron show extremely high performance, e.g., 20-nm resolution, but with more restrictions on maximum sample size, e.g., 50–100 μm. Here, it is important to highlight that the maximum sample size for hard X-ray tomography may be several orders of magnitude larger than in transmission electron microscopy (or electron tomography), due to
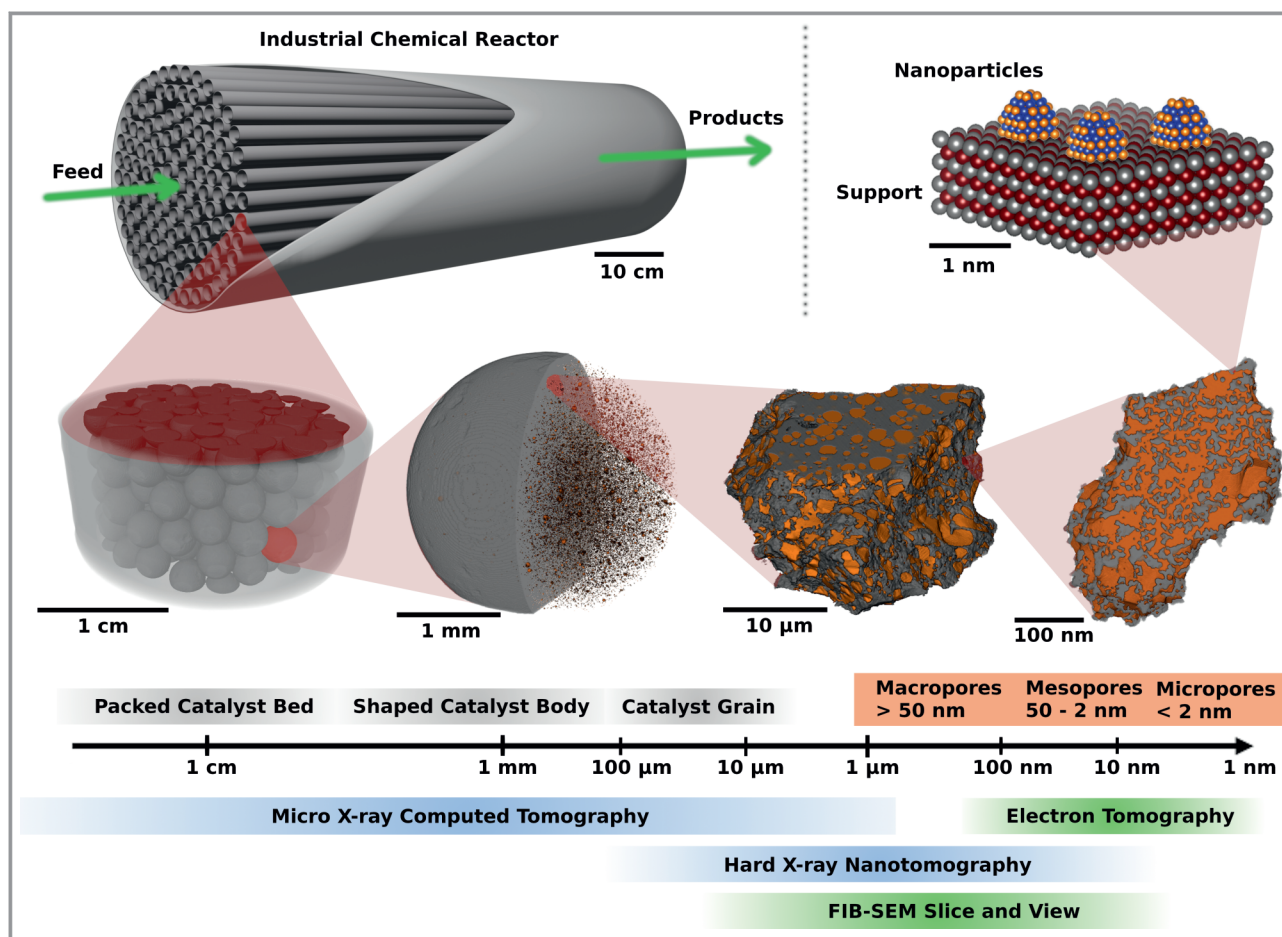
Figure 2. Illustration of the different relevant length scales in heterogeneous catalysis ranging from the reactor scale (m) down to the atomic scale (sub-nm). The four presented tomograms (bottom row) are from different sample sizes of the same Ni/Al$_2$O$_3$ reference catalyst batch (SPP2080-IMRC). The highlighted volume in each tomogram illustrates the approximate sample size of the subsequent imaging method, moving from lower (μm) to higher (nm) resolution. Volume renderings show the distinction between solid material and pores following image segmentation. Note: while the same catalyst batch was taken, the same exact sample, i.e., correlative imaging, was not measured each time, figure is for illustrative purposes only. Original work. Copyright © 2022 the authors.

higher attenuation of electrons in solid matter compared to hard X-rays.

Fig. 2 focuses on combined tomography methods to study different pore sizes in a solid catalyst, according to the IUPAC definition of macro- (> 50 nm), meso- (50–2 nm), and micropores (< 2 nm) [27]. In this overview example, the required methods may include X-ray microtomography (μ-XCT), hard X-ray nanotomography, focused ion beam scanning electron microscopy (FIB-SEM, also known as slice-and-view), or electron tomography (ET). Various combinations of these have been applied for a range of different catalyst materials, with literature studies typically ranging from the pellet scale down to the level of catalyst mesopores [26, 28–34]. This section reviews selected examples of catalyst systems analyzed by multiscale tomography methods and the information retrieved. This mainly focuses on hard X-ray tomography to cover all length scales ranging from the reactor down to single grains. As a reminder, the specific resolution and length scales in this section should not be

taken as hard limits since the experimental capabilities of synchrotron hard X-ray tomography are constantly improving [35, 36].

2.1 Reactor-Scale Imaging

Hard X-ray tomography studies applied to the reactor scale are mainly limited to μ-XCT. Tomography at the reactor scale is especially interesting for chemical engineering purposes related to mass and heat transport. For example, Caulkin et al. scanned different packed-bed reactors with inner diameters up to 29 cm by μ-XCT [37]. This allowed to retrieve information about the bulk density, local packing density profiles, pellet orientation, or particle-particle and particle-wall interactions. This information can be used to validate and improve simulation models for various reactor packings. Similarly, von Seckendorff et al. studied the void space in packed-bed reactors of spherical pellets and

analyzed the influence of the bed packing and bed porosity on the reactor pressure drop [38]. At reactor scale, µ-XCT has also found several applications in the design and analysis of monolithic reactors. For example, Ou et al. used µ-XCT to characterize the macroscopic porosity and tortuosity of SiC foam ceramics [39]. Such results can be applied to simulate mass transport, as shown by Kočí et al. for coated catalytic filters applied in exhaust gas aftertreatment [40]. In this case, the tomography data was transformed into mathematical mesh data and directly used for simulation studies, e.g., in OpenFOAM. Similarly, Bianchi et al. used µ-XCT measurements to retrieve 3D models of aluminum open foams for simulation of heat transport, with a special focus on heat transport processes between the foam and reactor walls [41, 42]. Sponge-like foams with different sponge materials for CO_2 methanation have also been studied using µ-XCT by Sinn et al. and have been combined with CFD simulation of heat transport based on the tomographic models [43]. CFD simulation results based on µ-XCT were additionally verified with magnetic resonance velocimetry studies by Sadeghi et al. [44].

As evident from the previous examples, µ-XCT represents one of the more common and applicable methods to study chemical reactors and larger structured materials. The appeal of this approach is clear, as it allows physical visualization of, e.g., reactor packing, which would otherwise be generated in an approximate manner by simulations. It should be noted that synchrotron hard X-ray tomography is the most feasible way to study large objects in a reasonable timescale, due to orders of magnitude difference in brilliance between synchrotron and laboratory X-ray sources.

2.2 Pellet-Scale Imaging

Some of the first reported X-ray tomography experiments in catalysis were performed on the pellet scale, tracing back to studies of olefin polymerization catalysts in the early 1990s by Conner et al. [45] and Ferrero et al. [46]. Generally, µ-XCT applied on the catalyst pellet scale is a powerful tool for analysis of morphological and textural properties. While catalyst pellets can in principle be studied by SEM or FIB-SEM sectioning, µ-XCT clearly offers high resolution visualization of larger samples in a comparably short timescale. For example, Hofmann et al. investigated single channels (mm scale) of a Pt/Al_2O_3 washcoated monolith for exhaust gas aftertreatment, following application of different hydrothermal aging conditions [47]. In this case, µ-XCT could reveal the formation of µm-sized Pt particles depending on the aging duration, including their distribution in 3D space within the monolith. Kaltner et al. also studied exhaust gas catalysts for NO oxidation based on hollow sphere alloy structures washcoated with Al_2O_3 [48]. Single spheres were studied with µ-XCT, while complementary neutron tomography was performed for a packed bed

of the catalysts. The above examples illustrate how shape and morphology, deactivation processes, and structural integrity are all feasible applications of µ-XCT on the pellet scale.

Catalyst synthesis can also be studied using µ-XCT on the pellet scale. For example, catalyst impregnation and the distribution of the impregnation solution or the deposited metal can be revealed in whole catalyst bodies. This was shown by Grunwaldt et al. for the impregnation of γ-Al_2O_3 pellets with $CuCl_2$ solution, revealing an impregnation gradient as a function of time based on the presence of Cu in the tomograms [17]. Similarly, Gibson et al. used µ-XCT to reveal the location of Mo after incipient wetness impregnation of γ-Al_2O_3 pellets with ammonium heptamolybdate [49]. They could show that addition of H_3PO_4 led to uniform impregnation profiles, while impregnation without the acid resulted in formation of Mo concentration hotspots. An intended impregnation gradient could be confirmed for Fe-Ni species after impregnation of γ-Al_2O_3 spheres by Silva et al. [50]. They synthesized a range of eggwhite, egg-shell, and uniform distributions depending on different impregnation parameters, with the distribution of impregnated metal species revealed by µ-XCT. They found that an egg-shell distribution is beneficial compared to the others in application for NH_3 decomposition.

For each of these examples, µ-XCT provided valuable information about morphological and textural properties as well as absorption gradients related to different chemical compositions or elemental distributions on the pellet scale. However, hard X-ray tomography with absorption contrast is difficult to analyze in a truly quantitative fashion, particularly at lower resolution, i.e., µm scale. For example, µ-XCT is generally unsuitable for porosity characterization as illustrated in Fig. 2, since porosity is typically defined on nm scale. Our recent study of porosity in the Ni/Al_2O_3 SPP2080-IMRC reference catalyst followed a multiscale approach including µ-XCT for analysis of single catalyst pellets (Fig. 3) [26]. In this case, µ-XCT carried out on a single particle (2.5 mm diameter, 2 h scan duration) only revealed 0.7 % macroporosity, which was homogeneously distributed in the catalyst pellet volume. However, complementary nanotomography and porosimetry studies calculated the overall macroporosity at ca 24 %. This shows the importance of employing additional tomography studies with higher resolution, i.e., X-ray nanotomography, depending on the specific science case.

2.3 Grain-Scale Imaging with X-Ray Nanotomography

Several different X-ray nanotomography methods are currently available to characterize catalysts with resolution of 100 nm and below. Typically, these techniques are limited to investigations of single catalyst grains with sample sizes of tens to hundreds of µm (see Fig. 2). Two particularly nota-
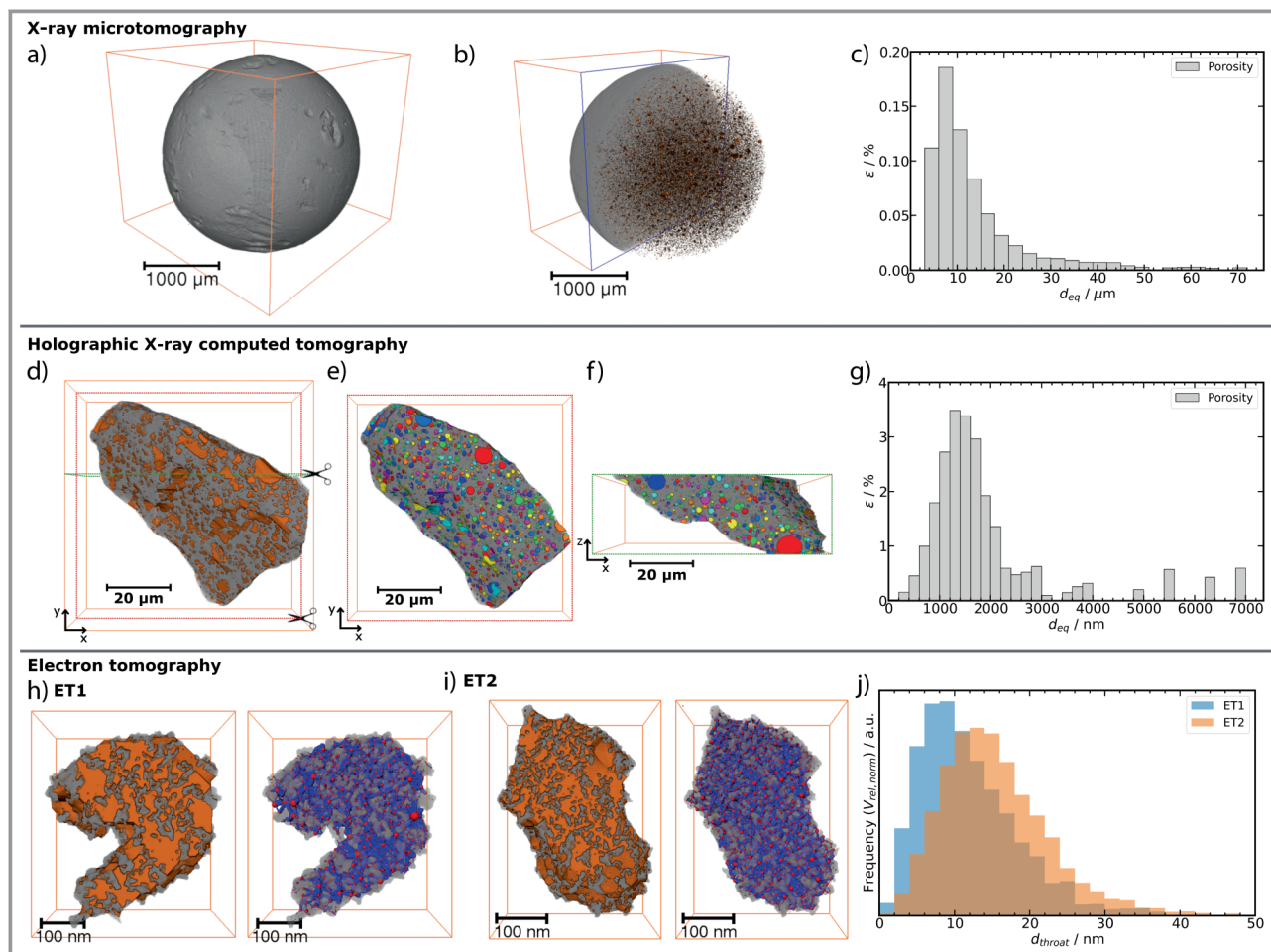
Chem. Ing. Tech. **2022**, 94, No. 11, 1–21

© 2022 The Authors. Chemie Ingenieur Technik published by Wiley-VCH GmbH

www.cit-journal.com

Figure 3. Characterization of the pore structure of the SPP2080-IMRC catalyst by a–c) X-ray microtomography (μ-XCT), d–g) holographic X-ray computed tomography (HXCT), and h–j) electron tomography (ET). Each segmented tomogram is shaded to represent the solid material and different pores. Porosity-weighted pore size distributions are shown based on image analysis. Reprinted from [26], under the terms and conditions of the Creative Commons CC BY-NC 4.0 license. Copyright © 2022 the authors.

ble nanotomography methods demonstrated for catalysis applications are ptychographic X-ray computed tomography (PXCT) and holographic X-ray computed tomography (HXCT). Ptychography, and its 3D counterpart PXCT, are phase contrast imaging methods more specifically known as scanning coherent diffraction imaging [51]. Ptychography and PXCT operate without an objective lens (between sample and detector) and utilize an iterative phase retrieval algorithm to recover the amplitude and phase of a highly oversampled object. Notably, this can lead to extremely high spatial resolution which is not limited by the focused beam size (as in conventional scanning probe imaging), and which is quantitatively sensitive to the electron density of the sample. HXCT is also a phase contrast imaging method but uses a full-field illumination, i.e., a beam size equal to or larger than the sample [52]. It is a propagation-based imaging technique which is used to obtain phase contrast images of the sample. HXCT is also notable for its high spatial resolution and ability to measure large objects in a shorter time due to the use of a larger full-field X-ray beam.

For the SPP2080-IMRC catalyst previously introduced above, HXCT was performed on a sample size of 50 μm diameter with a resolution of about 50 nm (Fig. 3) [26]. This revealed the macroporosity of ca 24 % that could not be found previously either by μ-XCT or conventional porosimetry, i.e., N$_2$ sorption and Hg porosimetry. This demonstrates a simple and elegant advantage of hard X-ray nanotomography over conventional pore characterization methods. In fact, the characterization of macropore structures within individual catalyst grains is an important application field of X-ray nanotomography. For example, da Silva et al. studied cylindrical samples of a fluid catalytic cracking (FCC) catalyst with a diameter of 8 μm by PXCT with a resolution reaching 39 nm [53]. They compared multiscale PXCT and μ-XCT porosity analysis with conventional Hg porosimetry, showing that a combination of both was required to study macropore and large mesopore length scales. Addressing smaller length scales, Fam et al. studied a model catalyst system based on hierarchical nanoporous gold by complementary PXCT, FIB-SEM slice and view, and

www.cit-journal.com

© 2022 The Authors. Chemie Ingenieur Technik published by Wiley-VCH GmbH

Chem. Ing. Tech. **2022**, *94*, No. 11, 1–21

ET [31]. They achieved a resolution of 23 nm with PXCT and could present advantages compared to FIB-SEM serial sectioning, especially regarding scanning time and the non-destructive nature of PXCT. By combining hard X-ray nanotomography with FIB-SEM and electron tomography, virtually the whole meso- and macropore space could be analyzed. Similarly, Becher et al. studied the influence of hydrothermal aging on Pt/Al_2O_3 catalysts by μ-XCT, PXCT, and ET focusing on differences in porosity [30]. In a recent study on hierarchically porous Ni/Al_2O_3 catalysts, we highlighted the importance of combining PXCT and ET to study the full meso- and macropore space [32]. Furthermore, the combination of both could reveal the true pore hierarchy in terms of multimodal pore size distribution, a distinction that is often difficult by conventional pore characterization. At even smaller length scales, Weissenberger et al. showed how the combination of PXCT and ET allows to study the hierarchical pore structure of single zeolite grains containing connected macropores with spatial resolution of 47 and 34 nm, respectively [34].

Of the currently operating nanotomography methods, PXCT is particularly interesting in materials and catalysis research not only for its extremely high spatial resolution but also due to the ability to recover quantitative information about the local electron density of the sample, i.e., number of electrons per unit space. Combined with additional structural information, i.e., elemental composition, X-ray density from a determined crystal structure, or skeletal density from He pycnometry, electron density can be used to interpret and quantify features such as catalyst mesoporosity. This is applicable even if such features are below the spatial resolution of the measurement, as shown

recently for the hierarchically porous Ni/Al_2O_3 SPP2080-IMRC catalyst [54]. Furthermore, electron density information might be applied to detect and localize coking as recently shown for an artificially coked Ni/Al_2O_3 catalyst by PXCT [55], and similarly for an FCC catalyst particle by Veselý et al. using HXCT [56]. This illustrates that electron density data from PXCT or HXCT might allow for a certain chemical sensitivity, in addition to high spatial resolution. For example, Ihli et al. studied 30-μm diameter cutouts of FCC catalyst particles by PXCT with a spatial resolution of 35 nm, subsequently assigning pore, clay, and zeolite phases in the tomograms based on the quantitative electron density observed [57]. In follow-up studies, they performed multiple PXCT measurements around the Fe K absorption edge, also called resonant PXCT, which allowed for additional chemical sensitivity and even visualization of local Fe distribution with extremely high spatial resolution of 39 nm as shown in Fig. 4 [58]. Further examples of advanced X-ray tomography methods allowing for chemical sensitivity are presented in Sect. 3, bridging the border between multiscale tomography and tomography with chemical contrast.

2.4 Electron Tomography for Highest Resolution

While hard X-ray nanotomography methods are approaching a resolution of 10 nm [35], this is not sufficient to resolve the whole mesopore space as illustrated in Fig. 2, which requires higher resolution analysis by ET. Suggested reviews on ET in catalysis provide some context for the present work [59–61]. ET can generally be applied to study mesopores in combination with X-ray tomography, as
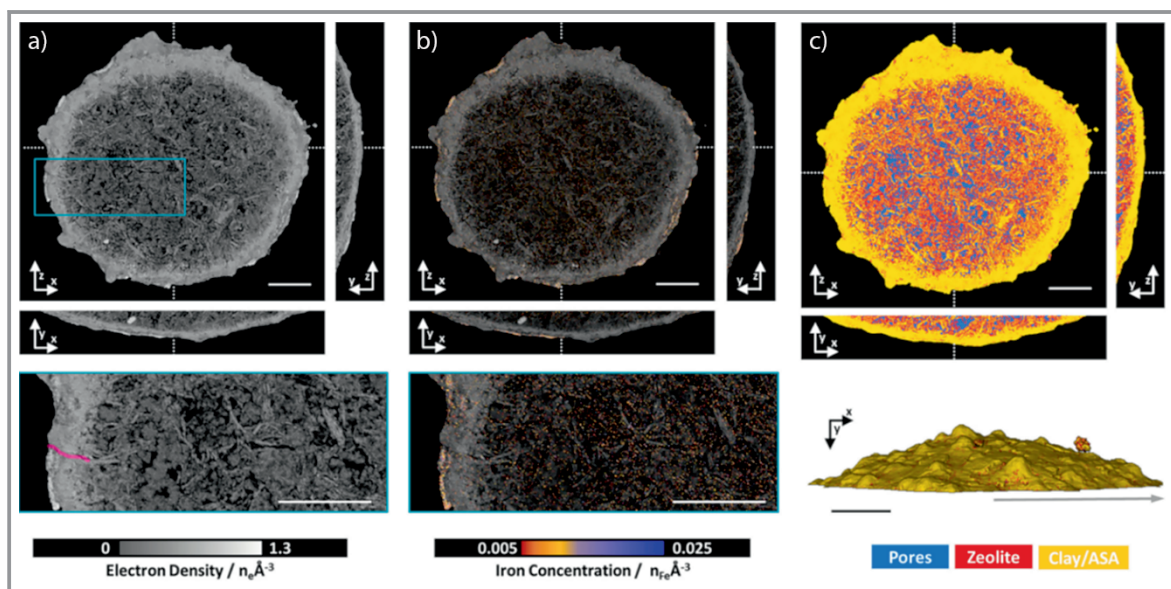

Figure 4. PXCT of a deactivated FCC catalyst. a) Slices of the measured electron density tomogram, with b) iron distribution overlaid. c) Tomogram following image segmentation, highlighting the distribution of the main catalyst components including pores, zeolite, and clay. All scale bars are 5 μm. Adapted from [58], with permission from the American Chemical Society. Copyright © 2018 American Chemical Society.

shown in several previous examples [30–34, 62]. Furthermore, ET can be applied to study the location of metal nanoparticles inside porous catalyst structures, as shown for Ni or Cu nanoparticles inside SBA-15 by Daoura et al. [63] and Prieto et al. [64], respectively. However, the use of ET in isolation may raise questions concerning representativeness, particularly for solid catalysts with significant structural heterogeneity. This is due to strict limitations on sample size when using electrons as the probe. Hard X-rays are therefore an excellent complementary tool, allowing to study much larger and, therefore, more representative samples.

3 Hard X-Ray Tomography for Chemical Imaging in Heterogeneous Catalysis

Chemical imaging refers to visualizing the spatially resolved chemical composition of materials. In addition to multiscale tomography as discussed in Sect. 2, hard X-ray tomography methods are broadly applicable for chemical imaging of catalytic systems, and therefore, help unravel their complex structural properties [8, 22, 23]. Such studies are possible thanks to the various interactions of hard X-rays with solid matter (summarized in Fig. 1), leading to a range of imaging contrast modes [20]. Relevant 3D chemical imaging of catalytic systems can, e.g., be performed by:

– spectroscopic imaging using XAS tomography (XAS-CT) to study changes in local atomic and electronic configuration, such as metal oxidation states or coordinating atoms.
– element-specific 3D mapping using XRF tomography (XRF-CT) to obtain spatially resolved and element-specific compositional data, such as metal distribution in a catalyst.
– powder XRD tomography (XRD-CT) to investigate material crystallite size and crystal structure.
– phase contrast imaging such as PXCT or HXCT to provide chemical information based on electron density, particularly for weakly absorbing samples.

A key function of chemical imaging is to derive local catalyst composition across multiple length scales. It is important to note that when combined with hard X-ray tomography, many common X-ray analytical tools such as XAS or XRD can effectively be extended into 3D space (Fig. 1b). Or from another perspective, many of the multiscale X-ray tomography tools outlined in Sect. 2 can additionally be combined with a chemical contrast mode. Overall, this provides a rich and often unique source of characterization data which cannot be feasibly obtained using alternative contemporary methods.

The chemical imaging approach can be applied in various branches of catalysis research, such as understanding catalyst synthesis [54], technical catalyst preparation [65], evaluating 3D spatial distribution of chemical constituents following synthesis [50], and in rationalizing catalytic activity

data through understanding of structural composition. 3D chemical imaging with hard X-ray tomography is also highly useful in understanding catalyst deactivation, even by post mortem or ex situ studies [56, 57]. For many well-known catalyst deactivation pathways including thermal degradation, sintering, poisoning, or pore blockage, chemical imaging with hard X-ray tomography has already been demonstrated as a uniquely powerful characterization tool. Further application of in situ and operando methodology combined with chemical imaging is also possible, as discussed mainly in Sect. 4.

In this section, important scientific advances achieved by hard X-ray tomography using several industrially relevant catalytic processes are elaborated. The chemical composition mapping of these catalysts and its influence on understanding material properties are demonstrated using a range of X-ray tomography methods.

3.1 Fragmentation of Olefin Polymerization Catalysts

Ziegler-Natta catalysts for production of polyolefins are widely used in chemical industry. During olefin polymerization, the catalyst experiences considerable mechanical stress due to polymer formation within the pores. This leads to fragmentation of virtually the entire catalyst particle by various mechanisms, making it an ideal case study for 3D chemical imaging. Attempts to classify the fragmentation behavior and the impact on catalyst performance and selectivity are of particular interest. By combining PXCT with XRF-CT as shown in Fig. 5, Bossers et al. studied the fragmentation behavior of a single Ziegler-Natta catalyst particle with a diameter of ca 40 µm, following a short treatment under reaction conditions [66]. Measurements were performed at 12 keV, achieving sub-micron resolution of 400 and 600 nm for PXCT and XRF-CT, respectively. In this case, PXCT visualized the entire catalyst body, acting as a canvas on which XRF-CT could isolate and locate elemental distribution of Ti and Cl species within the particle. In this case, $TiCl_4$ constitutes the active site precursor, therefore, by mapping Ti distribution, the authors could calculate the expansion of Ti species from the center of the particle and the related radial distribution of active sites. Following this proof of principle, Bossers et al. later extended this characterization to include more than 400 individual Ziegler-type catalyst particles for polyethylene production in a single high-resolution tomography measurement [67]. They performed PXCT of particles filled in a polyimide capillary with a diameter of 140 µm, achieving spatial resolution of 74 nm with a scan duration of 22 h. Here, electron density measurements were used to assess the degree of fragmentation within the particles based on volume, spherical diameter, and other physical parameters. Formation of high-density polyethylene could be correlated to the fragmentation behavior even by direct visualization of its formation

around the exterior of the particle. In a further study, high resolution HXCT was applied by Werny et al. on a silica-supported hafnocene-based catalyst to study the effect of ethylene polymerization on the catalyst structure [68]. Here, a series of particles were studied ex situ following 0 to 60 min under reaction conditions, allowing to distinguish changes in macroporosity, structural composition, and fragmentation behavior. This allowed a quantitative analysis of the catalyst pore network, including the distribution of silica-dominant and polymer-dominant regions as a function of reaction time.
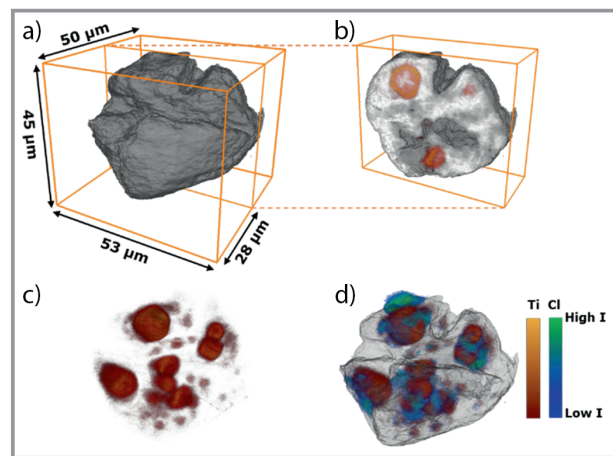

Figure 5. a) Reconstructed 3D volume rendering of a propylene polymerized Ziegler-Natta catalyst particle (~41 μm diameter). b) Extracted volume showing position of Ti species within the polymer-catalyst composite particle. c) Elemental distribution of Ti species. d) Elemental distribution of Ti and Cl within the composite particle. Reproduced from [66], under the terms and conditions of the Creative Commons CC BY-NC-ND 4.0 license. Copyright © 2020 American Chemical Society.

Olefin polymerization catalysts provide a strong example of the versatility of hard X-ray tomography, showing that multiscale imaging and chemical imaging are not mutually exclusive, rather they can be easily combined. This provides a combination of high resolution structural and chemical information in a single measurement. The greater depth of information, improved sample throughput, and greater measurement efficiency with hard X-ray tomography is clearly demonstrated compared to cross-sectional electron microscopy methods such as FIB-SEM, which are commonly used to study such catalysts.

3.2 Deactivation Pathways of Fluid Catalytic Cracking Catalysts

FCC catalysts are a typical example where catalyst deactivation can follow several pathways. This includes metal poisoning during cracking of heavy crude oil fractions into lighter hydrocarbons, followed by coke deposition and catalyst pore blockage, along with physical abrasion of catalyst

particles within the mobile fluidized catalyst bed [69–71]. Aside from reduced catalyst performance, understanding and deconvoluting these effects is challenging using conventional characterization tools. Employing hard X-ray tomography techniques with chemical contrast can help to visualize numerous effects in FCC particles, including changes in pore structure, metal poisoning, and chemical composition. This rich variety of physicochemical effects linked to the local catalyst structure has led to FCC catalysts being one of the few relatively well-studied examples using hard X-ray tomography.

Among the first hard X-ray tomography studies on degradation of a single FCC catalyst particle was the work by Ruiz-Martínez et al. using a combination of XRF-CT, XAS-CT, and XRD-CT [72]. The presence of Ni and V species as contaminants originating from crude oil was detected using XRF-CT. This allowed to map the distribution of such metal poisons in a single measurement, revealing an egg-shell distribution of Ni. A comparatively more uniform distribution of V was observed across the particle. However, X-ray attenuation effects during XRF-CT made it difficult to conclude the distribution of V within the FCC particle. The local oxidation state of these metal species could be recovered by complementary XAS-CT, giving insight into the specific interaction of the contaminant metals with the support. This information was complemented by XRD-CT to identify regions of crystalline phases in the particle, and the transformation of these, e.g., zeolite dealumination and destruction, between a fresh and aged particle. Correlating these results revealed a connection between the metal poisoning and zeolite destruction effects. Combining a multiscale and multimodal chemical imaging approach, Bare et al. also studied the structure and chemical composition of spent FCC catalyst particles [73]. Synchrotron μ-XCT was performed at 15 keV to image hundreds of particles and identify different shapes, sizes, and presence of internal voids or very large macropores. Selected particles (two of diameter 50–70 μm and two of diameter 250–390 μm) were then measured with high-resolution hard X-ray nanotomography at 8 keV to obtain images with a voxel size of ca 40 nm. This was complemented by micro-XRF and XRD mapping in 2D and provided a qualitative correlation of specific metal poisons and zeolite degradation. This approach was later expanded by Kalirai et al. who used XRF-CT to map a broad range of deposited metal impurities (Fe, Ni, V, Ca) as well as catalyst constituents (La, Ti) with submicron voxel size (resolution of ca 1.4 μm) and high chemical sensitivity [74]. As shown in Fig. 6, this allowed to identify correlation between specific metal poisons, indicating the presence of different deposition mechanisms based on penetration depth within the particle. For example, while Fe, Ni, and Ca were found to aggregate at the particle exterior, Ni and V typically penetrated further. Analysis of two catalyst particles (ECAT1 and ECAT2) aged for consecutively longer duration showed an increase in metal deposition as a function of aging time.
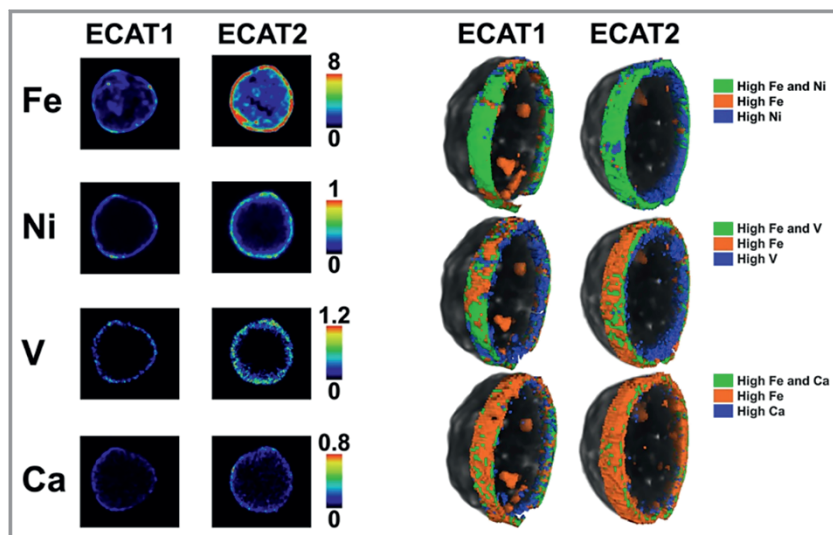
Figure 6. 2D slices of Fe, Ni, V, Ca XRF signals showing distribution of each species within the ECAT1 and ECAT2 FCC catalyst particles. The scale bar intensity indicates increasing amount of each species. 3D volumes represent regions of high concentration and indicate correlation between specific metal pairs. Adapted from [74], under the terms and conditions of the Creative Commons CC BY-NC 4.0 license.

From these early but still recent hard X-ray tomography studies, characterization efforts intensified on the FCC catalyst leading to several methodological breakthroughs. Meirer et al. were able to visualize individual large macropores with a voxel size of 70 nm (approximate resolution ca 200 nm) within an entire particle, including identification and location of specific metal poisons within individual pores [75]. The data were then exploited for gas permeability simulations, highlighting the natural intersection of 3D imaging data with modeling and simulation. The same group later expanded this approach using high resolution full-field hard X-ray tomography (spatial resolution ca 314 nm) to include a series of particles at different degrees of deactivation, quantifying pore features and metal deposition as a function of aging [70]. Further studies focused in more depth on specific poisons such as Ni [76] and even 3D visualization of relative degree of coking within single particles [56]. Furthermore, recent publications by Ihli et al. highlighted the effects of metal contamination on the pore structure by performing PXCT at a resolution of ca 35 nm to support pore network modeling of macro- and mesopores within spent FCC catalyst particles. This was complemented by XRD-CT and XRF-CT to again correlate presence of metals and study amorphization and degradation of zeolite domains [57]. Later, the same group used XAS-CT to map the specific location and chemical state of Fe contaminants within FCC particles [77].

3.3 Other Examples of Chemical Imaging

The rich chemistry and industrial importance of FCC catalysts has led to a strong focus on hard X-ray tomography studies with this system. However, this should not be interpreted as a limitation on the applicability of hard X-ray tomography in catalysis. On the contrary, it indicates great flexibility since hard X-ray tomography can address such a broad array of scientific questions even by itself, in turn providing a unique and rich source of data. A common feature of the previously reviewed case studies is that measurements were performed ex situ or under ambient conditions. However, the characterization potential of hard X-ray tomography can be extended even further to examine catalysts at work, as discussed in the following section.

4 In Situ and Operando Hard X-Ray Tomography of Catalysts at Work

In heterogeneous catalysis, the terms in situ and operando are used to define a characterization measurement as follows [78–80]:

- in situ: measurement performed under non-ambient conditions, e.g., high/low temperature, high/low pressure, presence of solvent and/or non-ambient atmosphere
- operando: subgroup of in situ measurement with the catalyst under working conditions, proven by product analysis which is ideally quantitative and shows conversion, yield, or selectivity, e.g., mass spectrometry and gas chromatography

Operando measurements are often more challenging but provide more valuable data. The goal of most operando studies is to simultaneously probe the catalyst structure and the corresponding catalytic activity to establish structure-activity relations. Operando methodology has been firmly established over the last two decades as one of the most important developments in modern catalyst characterization, being applied to a wide range of spectroscopy and diffraction methods [81–85]. Given the powerful capabilities of hard X-ray tomography for structural and chemical characterization, performing such experiments under working conditions would effectively allow visualization of structure-activity relations in 3D space; in other words, to make a movie of catalysts at work as discussed by Meirer and

Weckhuysen [19]. However, despite excellent potential, the field of operando hard X-ray tomography is still relatively unexplored in catalysis.

Unlike multiscale tomography and chemical imaging, which have evolved in dependence on the technology level of synchrotrons, the limiting factor for operando studies is the availability of suitable sample environments (in situ/operando cells). Low awareness of hard X-ray tomography in catalysis is also a barrier to further development. In this context, the following section outlines notable developments of in situ and operando catalysis research using synchrotron hard X-ray tomography. Such studies have progressed in recent years from measuring single catalyst grains to large technical catalyst samples, combining multiple contrast modes in a single measurement, and with consistently better spatial resolution to extract maximum value from the measurements. The characterization power of hard X-ray tomography is only enhanced further by applying reaction conditions, leading to highly multidimensional studies.

4.1 Sample Environments for In Situ or Operando Hard X-Ray Imaging

Appropriate sample environments are essential for in situ and operando studies in catalysis. In situ cells typically allow heating and exposure to controlled gas environments. Operando cells must extend to realistic working conditions and include product analysis which is preferably quantitative. However, a compromise is typically made between characterization data quality and design of the operando cell compared to realistic catalytic operating conditions. The challenges of operando sample environments particularly for X-ray characterization were discussed by Meunier [86], Tsakoumis et al. [87], and Newton et al. [88]. Grunwaldt et al. further discussed these challenges specifically in the context of X-ray imaging [9]. The "perfect" operando cell would permit kinetically relevant conditions for meaningful observation of structure-activity relations, though such a setup has not yet been demonstrated for hard X-ray tomography.

Operando hard X-ray tomography is more experimentally demanding than both 2D imaging, e.g., electron microscopy, and comparable operando methods such as XAS, IR, or Raman spectroscopy, where in situ or operando cells are even commercially available. This is due to the unique geometric requirements of tomography, which requires free rotation while maintaining a suitable reaction environment. Furthermore, tomography studies generally require mechanical, e.g., vibrational, stability well below the desired resolution level. Since in situ and operando cells are typically custom-built for specific experiments, discussion of these is presented below with selected case studies.

4.2 In Situ Tomography of Catalysts under Non-Ambient or Working Conditions

Among the earliest examples of in situ hard X-ray tomography is the work from Gonzalez-Jimenez et al., who studied an iron oxide-based Ruhrchemie catalyst for Fischer-Tropsch (FT) synthesis [89]. A single 20-µm catalyst grain was loaded in a capillary reactor with a diameter of 100 µm and exposed to various conditions including 10 bar syngas ($H_2/CO = 1$) at 523 K. Similar to the FCC studies shown previously, here, XAS-CT was used to locate iron oxide species within the particle, while complementary in situ 2D microscopic XAS measurements could probe the oxidation state (Fe_2TiO_5, Fe_2O_3, and Fe_3O_4) of different clusters as a function of reaction time (spatial resolution 30 nm). Catalytic activity data was not recorded during tomography but later supplemented by laboratory experiments, due to rather demanding conditions of the FT to olefins process. Laboratory tests and X-ray imaging data were then combined to justify the catalytic performance and selectivity towards olefin synthesis. Cats et al. performed similar XAS-CT experiments on cobalt-based FT catalysts, this time exploring the spatial distribution and oxidation state of cobalt nanoparticles (spatial resolution 30 nm) under various conditions including 10 bar syngas ($H_2/CO = 2$) at 523 K [90]. It should be noted that only an operando approach can feasibly distinguish metal oxidation states in a working catalyst. Otherwise, such structures may not be stable or may not even form unless exposed to reaction conditions. Combined with X-ray tomography, this type of analysis can be performed in 3D space.

As the target of the previous studies was to obtain high spatial resolution, a small catalyst sample size, i.e., a single grain, was selected. Later work by Price et al. extended the in situ hard X-ray tomography approach to small packed-bed capillary reactors (diameter 400 µm) [82]. A multimodal chemical imaging study was performed by combining XRF-CT, XRD-CT, and XAS-CT at 13 keV on two model Co/SiO_2 FT catalysts including Re promoters and Ti-modified supports. Online mass spectrometry was used to identify but not quantify product distribution, which was later supplemented by laboratory tests. In this case, XRD-CT was used to monitor crystallite size of active Co species as well as oxidation state. The Ti-modified catalyst was found to be resistant to CoO formation and metal sintering, therefore retaining higher selectivity for C_5 and larger hydrocarbons. It is important to note that 3D spatially-resolved XRD-CT as applied here is sensitive to local chemical composition in 3D space. This could reveal minority phases which may not be visible to conventional bulk XRD analysis and even locate these within the catalyst particle. By extension, an in situ hard X-ray tomography approach using XRD-CT is uniquely capable of retrieving such data on minor phase changes and relating them to catalyst performance.

A further notable development for in situ tomography was presented by Vamvakeros et al., who measured a

catalytic membrane reactor for oxidative coupling of methane to ethylene [91]. This larger technical catalyst system consisted of a 2.4-mm diameter hollow-fiber BaCoFeZrO membrane packed with $MnNaW/SiO_2$ powder catalyst and placed within a quartz reaction tube. The reactor was exposed to a flow of up to 5 vol % CH_4 in He (100 mL min^{-1}) through the reactor and air (100 mL min^{-1}) at the outer membrane. A mass spectrometer capillary at the reactor outlet was used to monitor the reaction feed, which was otherwise left open to ambient air to allow free rotation for tomography. The catalyst was found to be active although quantitative conversion data was not shown. In this example, XRD-CT with a resolution of ca 20 μm was used to monitor crystalline phases and changes in phase distribution in 3D space, as shown in Fig. 7. For example, crystalline Na_2WO_4 and Mn_2O_3 observed at room temperature were almost completely removed up to 1048 K, while $BaWO_4$ formed at the interface between the catalyst and membrane wall. In a single measurement this demonstrates how in situ XRD-CT can be used to distinguish active and spectator species, along with identifying stable and unstable phases. Location of crystalline phases in 3D space allows to observe differences in behavior based on position in the reactor. This can be used to observe and rationalize catalyst deactivation in larger technical systems. Notably, this serves as one of the earliest tomographic solid-state investigations of an active catalyst resembling a technical application scale, while XRD tomography is generally applicable for virtually any catalytic material with crystalline components.

A recent study by Fjellvåg et al. used in situ μ-XCT to study grain reconstruction of Pd and Pd/Ni wires used during NH_3 oxidation for synthesis of nitric acid [92]. This reaction is topical in terms of sustainability as it involves significant loss of noble metal during operation. The Pd-based wires are used as a downstream catchment material during decomposition of Pt-based wire catalysts. Both types of wires rapidly change from a smooth exterior in the fresh wire to a characteristic cauliflower-like structure under the harsh reaction conditions of NH_3 oxidation (1073–1223 K, 1–12 bar $NO_x/NH_3/H_2O/O_2$). Both fresh and pre-aged catalyst wires were placed in a capillary reactor downstream of several Pt wires. The reactor was heated to 1273 K in synthetic air, while the Pd wires were continuously studied by in situ tomography, with an acquisition rate of 1 tomogram in 10 s. This allowed to monitor the surface and bulk reconstruction behavior of the wires under oxidative conditions, as shown in Fig. 8. It should be noted that here synthetic air was used to stimulate for-

mation of gas-phase PtO_2, which is proposed to account for the Pt loss mechanism. This constitutes a model in situ reaction condition rather than a relevant condition for NH_3 oxidation. Chemical composition of the wires was supported by complementary SEM-EDX analysis of single wire cross sections. As shown in previous examples, acquiring chemical composition from μ-XCT data could be feasible, covering extended length scales more efficiently than would be possible with SEM-EDX.
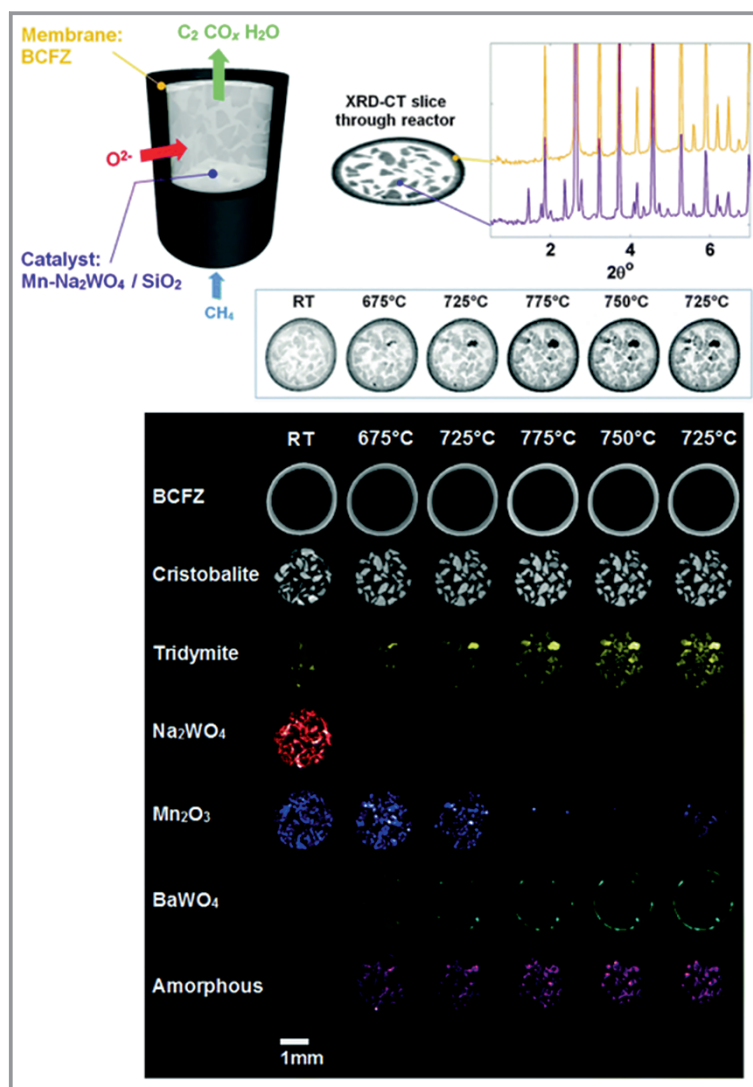

Figure 7. Illustration of the catalytic membrane reactor and cross-sectional XRD-CT data as a function of temperature. Images can be deconvoluted based on selected Bragg reflections, showing the location and composition of the membrane material (BCFZ), various crystalline phases, and amorphous signals. Reproduced from [91], under the terms and conditions of the Creative Commons CC BY 3.0 license. Copyright © 2015 The Royal Society of Chemistry.
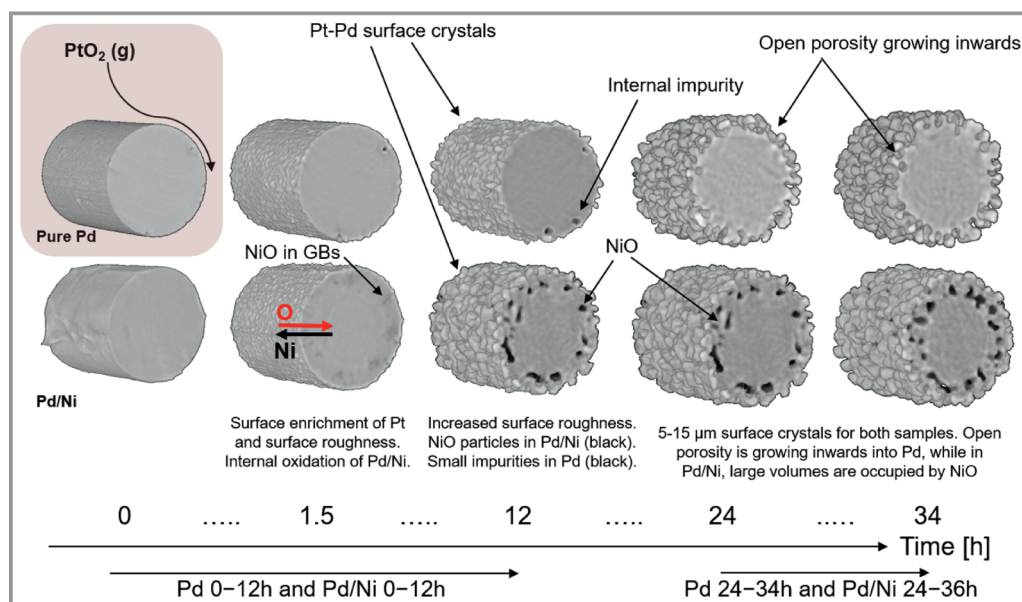
www.cit-journal.com

© 2022 The Authors. Chemie Ingenieur Technik published by Wiley-VCH GmbH

Chem. Ing. Tech. **2022**, *94*, No. 11, 1–21

Figure 8. In situ μ-XCT of morphological changes and chemical dynamics of Pd and Pd/Ni (91.3/8.7 at %) wires during experiments in synthetic air at 1273 K. Reprinted from [92], with permission from Elsevier. Copyright © 2022 Elsevier.

4.3 Towards Operando Tomography with Quantitative Catalytic Performance Data

Significant progress has been made in recent years towards operando tomography of catalysts at work, most notably with the XRD-CT methodology outlined in previous examples. One focal area has been in catalytic partial oxidation of CH_4 to syngas, where Vamvakeros et al. performed 5D operando imaging to obtain detailed 3D structural analysis via XRD-CT of a Ni/Pd catalyst supported on CeO_2-ZrO_2/ Al_2O_3 [84]. The study was performed under various reaction conditions, while XRD-CT data was acquired on reasonable time frames (< 2 min per tomogram slice) allowing to study physicochemical changes, potentially also dynamic changes. The data were of sufficient quality to allow Rietveld analysis, therefore enabling precise interpretation of Ni crystallite size, differentiation between four different $Ce_xZr_yO_2$ species, and the chemical evolution of the catalyst. Although quantitative performance data was not shown, mass spectrometry was used to follow and confirm the desired gas environment at each reaction step. Nevertheless, this study constitutes a significant breakthrough in moving beyond basic 3D phase identification by XRD-CT towards meaningful crystallographic analysis. In this case, the so-called 5D operando imaging implies three spatial dimensions from tomography, one scattering dimension from XRD, and a further dimension indicating the applied reaction conditions. Further studies in this field were performed by Matras et al. on a similar catalyst, Ni-Pd/CeO_2-ZrO_2/Al_2O_3, which included an analysis of coke deposits as a function of reaction conditions [93]. They found the formation of catalytically active Ni-C

species during high methane conversion in the activation step, which later converted to graphite under reaction conditions resulting in a decrease in activity and deactivation of catalyst by coking. Furthermore, CeO_2 was found to mitigate the coke deposition by acting as an oxygen storage medium, despite its inability to prevent sintering of Ni particles. Further studies by Vamvakeros et al., Matras et al., and Senecal et al., include oxidative coupling of methane in membrane reactors [94] and as fixed-bed powder reactors [95, 96] as well as total scattering studies of Co-based FT catalysts [97]. In most cases, the catalysts were studied under model reaction conditions, including detailed crystallographic analysis in 3D space with Rietveld refinement. These serve as an excellent demonstration of the power of hard X-ray tomography for unique structural characterization.

In an effort to ensure tight control over reaction conditions and quantify product analysis, our group recently described an operando hard X-ray tomography reactor for analysis of mm-scale technical catalysts, including an open discussion of design principles for others to reproduce and iterate on the design [98]. The reactor was first applied for operando XAS-CT of Cu-zeolite washcoated monolith catalysts for selective catalytic reduction of NO_x with ammonia (NH_3-SCR), currently an industry standard in automotive emissions control [81]. Tomography data was recorded around the Cu K absorption edge, revealing the local oxidation state and coordination environment of Cu species within the catalyst washcoat. At the same time, NO conversion to N_2 was quantified by online mass spectrometry. This approach revealed chemical gradients of Cu^+ and Cu^{2+} species within the catalyst as a function of temperature

(473–673 K), gas environment, and position within the catalyst washcoat (Fig. 9). These chemical gradients are linked to a complex interplay of factors such as reactant diffusion to the catalytic active sites, local reaction rate, and NH_3 inhibition at lower temperatures. As such, they provide for the first time a physical visualization of mass transport effects of gaseous reactants to the catalytically active sites, correlated to quantitative (although bulk) activity measurements. In this example, a section of a catalyst monolith was

used rather than catalyst powder, indicating applicability of the method for technical catalysts. The study also highlights an important distinction between operando spectroscopic measurements on model powders which operate under ideal plug-flow conditions and technical materials which can be affected by mass transport, gas bypass, and other physical parameters [99–101]. Furthermore, the chemical gradients observed are effectively a direct visualization of structure-activity relations in 3D space, which can be feasibly observed only with a combination of operando XAS and tomography. The same observations are demonstrably not possible with conventional bulk XAS analysis.

5 Conclusions and Future Perspective

This review outlines the state of the art in the relatively young and exciting field of synchrotron tomography for heterogeneous catalysis research. The central aim is to raise awareness of the current potential and future possibilities of hard X-ray tomography for advanced catalyst characterization. In this context, the review focuses strongly on specific experimental results which demonstrate the applicability of tomography to a broad audience. Three focal areas were identified and presented, covering the majority of currently known tomography literature: 1) multiscale imaging, 2) chemical imaging, and 3) in situ or operando imaging. While these topics are presented separately, there are in principle no strictly defined borders between the topics. For example, multiscale tomography (1) is often performed with multiple contrast modes (2), while in situ or operando measurements (3) can be found at different length scales (1) or contrast modes (2). Furthermore, this review limits its scope strictly to hard X-ray tomography performed at synchrotron light sources, which hold excellent future potential for studying heterogeneous catalytic systems. The use of free electron lasers (FELs), laboratory X-ray sources (micro- and nanoscale), soft X-ray microscopy, and correlative microscopy with electrons and X-rays are not covered here but are also active research areas. It should further be noted that, to solve particularly challenging problems in catalysis, a complementary approach based on multiple (imaging) methods is often essential. It is rare that hard X-ray tomography alone can provide all the answers, but on the other hand, hard X-ray tomography offers a unique source of 3D spatially resolved data which cannot be feasibly obtained by contemporary methods.

Several questions continually arise when presenting or discussing X-ray tomography in the catalysis community and with chemical industry. Many can be indirectly answered by remembering the golden rule of tomography (Fig. 1c), which is the balance between: 1) spatial resolution, 2) measurement time, and 3) sample size. A good rule of thumb is that a maximum of two parameters can be selected and optimized, and the third must be compromised. In this context, many tomography studies are planned with a
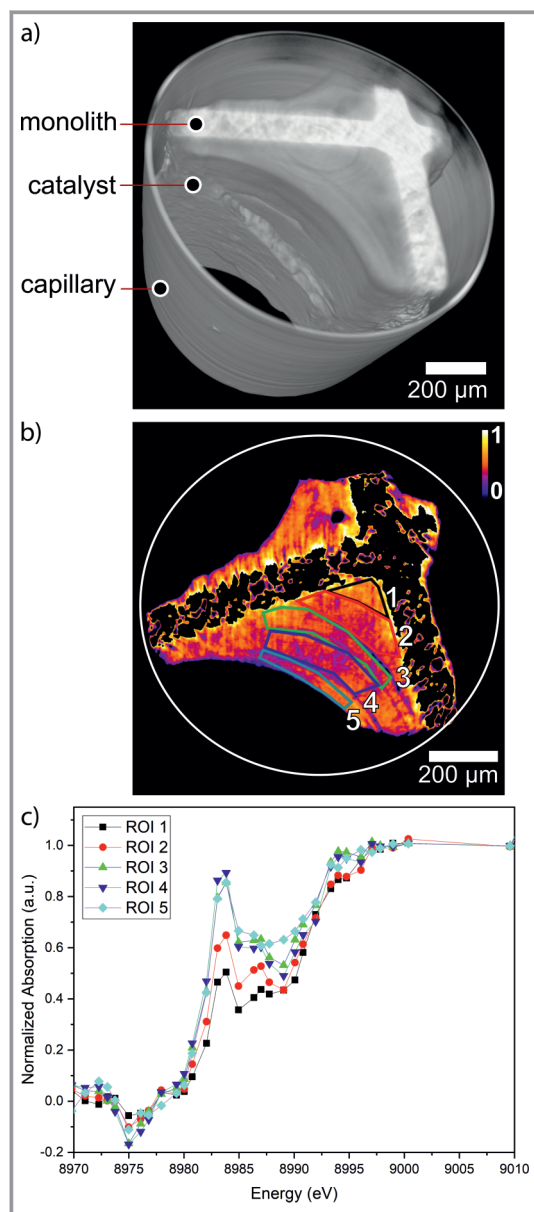

Figure 9. Chemical gradients in a Cu-SSZ-13 washcoat. a) Tomography reconstruction of a washcoated monolith sample in a 1-mm quartz capillary. b) Cross section of the catalyst measured under SCR conditions at 623 K showing areas of interest (ROI 1–5). c) Normalized XAS spectra from ROI 1–5, illustrating chemical gradients. Reprinted from [81], with permission from Springer Nature. Copyright © 2021 the authors.

specific goal in mind, such as maximum spatial resolution on a finely structured sample, maximum time resolution on a transient or sensitive sample, or maximum throughput imaging of many samples to generate statistically representative datasets.

– Spatial resolution: This parameter is selected based on experimental needs. For very large samples, e.g., mm- to cm-scale, microtomography is often sufficient to gain an overview on sample structure, integrity, or different components in a composite catalyst sample. For fine structural details, such as mesopore or macropore networks (< 100 nm scale), nanotomography is actively chosen. In terms of maximum spatial resolution, the best-performing hard X-ray nanotomography methods such as PXCT and HXCT have already almost exceeded the 10-nm limit in a little over 10 years since their invention. With future development of 4th generation synchrotron light sources, hard X-ray tomography is envisioned at single digit nm resolution [102]. Hard X-ray nanotomography is therefore expected in future to approach parity with electron microscopy in terms of spatial resolution, while exceeding the sample size limitations of electron microscopy by several orders of magnitude.

– Time scale: Tomography is often imagined to have slow acquisition speed (order of 1 tomogram in several minutes for microtomography, or 1 tomogram in several hours for nanotomography) due to the requirement to scan multiple rotational angles and positions to generate a single dataset. Therefore, it is often assumed that tomography is unsuitable for some transient or rapid chemical processes or the study of dynamic conditions. However, achieving good time resolution during tomography can be a deliberate choice during experiment design, often at the expense of spatial resolution or sample size (see the golden rule in Fig. 1c). For example, catalyst washcoating has been investigated in real time with a tomogram acquisition rate of 0.2 Hz [65], while beamlines optimized for time-resolved tomography can routinely operate at 20 Hz or faster [103]. This shows that tomography data can feasibly be acquired also for rapid or transient processes on the sub-second timescale if this is required for the experimental case.

– Sample throughput and representativeness: This concept can refer to measuring large sections of a single sample, e.g., a technical catalyst pellet or washcoated monolith, or measuring multiple smaller samples within a given time. In both cases, high throughput studies aim to facilitate statistically meaningful data analysis on the sample. This is important in heterogeneous catalysis due to high complexity of typical sample systems, e.g., the thoroughly studied FCC catalyst system. Microscopy and tomography studies with both electrons and X-rays are often questioned or criticized as being potentially unrepresentative of the material under investigation, due to limitations in sample size or number of samples which can be studied on a reasonable time scale. However, in terms of raw data volume which can be generated, hard X-ray tomography probably is among the higher throughput imaging methods in operation today. This is largely thanks to the high-quality and high-energy X-rays generated by modern synchrotron light sources. With the ability to measure large data volumes in relatively high throughput, hard X-ray tomography is arguably more representative in this context than any other known imaging technique, which is therefore ideal for the study of heterogeneous catalysis.

With respect to X-ray tomography, the experimental capabilities of modern synchrotron radiation sources are rapidly improving, while newer 4th generation synchrotrons are currently opening or are in development around the world [102, 104, 105]. The potential improvements in data quality, image resolution, and sample throughput for X-ray tomography studies are truly unprecedented and will be realized certainly within the next decade. In summary, due to broad applicability, experimental flexibility, and the unique data available, hard X-ray tomography certainly has a bright future in catalysis research.

Srashtasrita Das received her B.Tech. degree in Chemical Engineering in 2015 from National Institute of Technology Rourkela (India), and her Master's degree in Chemical Engineering in 2019 from Arizona State University (USA). During her M.Sc. she studied metal oxides for H_2O/CO_2 splitting and energy storage with Prof. Muhich. Since 2020, she is a Ph.D. student in the X-ray Microscopy group of Dr. Sheppard with Prof. Grunwaldt at the Institute for Chemical Technology and Polymer Chemistry at Karlsruhe Institute of Technology (Germany). Her current research focuses on in situ/operando characterization of catalysts using synchrotron-based hard X-ray microscopy.

Shweta Sharma received her M.Sc. in Chemistry in 2019 from Dr. Ambedkar at NIT (India). During her M.Sc., she explored applications of ionic liquids as surfactants and as catalysts for lignin depolymerization. Then, she worked at CSIR-NCL, Pune, India on heterogeneous catalysis for environmentally important reactions. Since 2021, she is a Ph.D. student in the X-ray Microscopy group of Dr. Sheppard with Prof. Grunwaldt at Institute for Chemical Technology and Polymer Chemistry at Karlsruhe Institute of Technology (Germany). Her research focuses on 3D spatial characterization of technical catalysts for emissions control with X-ray microscopy and tomography.

Reihaneh Pashminehazar is a postdoc researcher since 2019 in the X-ray Microscopy group of Dr. Sheppard with Prof. Grunwaldt at the Institute for Chemical Technology and Polymer Chemistry at Karlsruhe Institute of Technology (Germany). She received her Ph.D. in Process Engineering at Otto-von-Guericke University of Magdeburg (Germany) in the group of Prof. Tsotsas. Her thesis was about the morphological characterization of soft agglomerate produced in fluidized beds. The main focus of this characterization was based on microtomography imaging. Her main research activity is 3D image processing of tomography data obtained from laboratory or synchrotron sources.

Sebastian Weber received his B.Sc. and M.Sc. in Chemistry from Universität Leipzig (Germany) in 2015 and 2018, respectively. During his M.Sc., he studied plasma synthesis of mayenite electrides and potential applications in ammonia synthesis with Dr. Schunk (hte GmbH) and Prof. Gläser (Leipzig). Since 2018, he is a Ph.D. student in the X-ray Microscopy group of Dr. Sheppard with Prof. Grunwaldt at the Institute for Chemical Technology and Polymer Chemistry and Institute of Catalysis Research and Technology at Karlsruhe Institute of Technology (Germany). His research focuses on spatially resolved catalyst characterization with various hard X-ray contrasts on nickel-based catalysts.

Thomas Sheppard is a senior scientist (without tenure) at Karlsruhe Institute of Technology (Germany). He received his Ph.D. in Chemistry in 2014 from Queen's University Belfast (UK), followed by postdoctoral research with Prof. Grunwaldt at KIT from 2014–2017. He is a visiting scholar at Deutsches Elektronen-Synchrotron DESY since 2020 and at Hamburg University of Technology since 2021. He currently leads an independent research group focused on advanced catalyst characterisation with synchrotron radiation, mainly X-ray microscopy. His research interests include unconventional catalyst characterization tools, in situ/operando studies, and studying structure-activity relations.

Abbreviations

CFD	computational fluid dynamics
CT	computed tomography
ET	electron tomography
FCC	fluid catalytic cracking
FIB-SEM	focused ion beam scanning electron microscopy
FT	Fischer-Tropsch
HXCT	holographic X-ray computed tomography
IR	infrared
PXCT	ptychographic X-ray computed tomography
SCR	selective catalytic reduction
XAS	X-ray absorption spectroscopy
XAS-CT	X-ray absorption spectroscopy computed tomography
μ-XCT	microscale X-ray computed tomography
XPS	X-ray photoelectron spectroscopy
XRD	X-ray diffraction
XRD-CT	X-ray diffraction computed tomography
XRF	X-ray fluorescence
XRF-CT	X-ray fluorescence computed tomography

References

[1] *Handbook of Heterogeneous Catalysis* (Eds: G. Ertl, H. Knözinger, J. Weitkamp), 2nd ed., Wiley-VCH, Weinheim **2008**.

[2] P. Anastas, N. Eghbali, *Chem. Soc. Rev.* **2010**, *39 (1)*, 301–312. DOI: https://doi.org/10.1039/B918763B

[3] P. Lanzafame, S. Perathoner, G. Centi, S. Gross, E. J. M. Hensen, *Catal. Sci. Technol.* **2017**, *7 (22)*, 5182–5194. DOI: https://doi.org/10.1039/C7CY01067B

[4] E. Gallei, E. Schwab, *Catal. Today* **1999**, *51 (3)*, 535–546. DOI: https://doi.org/10.1016/S0920-5861(99)00039-5

[5] A. Cybulski, J. A. Moulijn, *Structured Catalysts and Reactors*, 2nd ed., CRC Press, Boca Raton, FL **2005**.

[6] S. Mitchell, N.-L. Michels, G. Majano, J. Pérez-Ramírez, *Curr. Opin. Chem. Eng.* **2013**, *2 (3)*, 304–311. DOI: https://doi.org/10.1016/j.coche.2013.04.005

[7] C. M. A. Parlett, K. Wilson, A. F. Lee, *Chem. Soc. Rev.* **2013**, *42 (9)*, 3876–3893. DOI: https://doi.org/10.1039/C2CS35378D

[8] B. M. Weckhuysen, *Angew. Chem., Int. Ed.* **2009**, *48 (27)*, 4910–4943. DOI: https://doi.org/10.1002/anie.200900339

[9] J.-D. Grunwaldt, J. B. Wagner, R. E. Dunin-Borkowski, *ChemCatChem* **2013**, *5 (1)*, 62–80. DOI: https://doi.org/10.1002/cctc.201200356

[10] K. A. Cychosz, R. Guillet-Nicolas, J. García-Martínez, M. Thommes, *Chem. Soc. Rev.* **2017**, *46 (2)*, 389–414. DOI: https://doi.org/10.1039/C6CS00391E

[11] C. Schlumberger, M. Thommes, *Adv. Mater. Interfaces* **2021**, *8 (4)*, 2002181. DOI: https://doi.org/10.1002/admi.202002181

[12] S. Bordiga, E. Groppo, G. Agostini, J. A. van Bokhoven, C. Lamberti, *Chem. Rev.* **2013**, *113 (3)*, 1736–1850. DOI: https://doi.org/10.1021/cr2000898

[13] T. Shido, R. Prins, *Curr. Opin. Solid State Mater. Sci.* **1998**, *3 (4)*, 330–335. DOI: https://doi.org/10.1016/S1359-0286(98)80041-7

[14] H. Kohlmann, *Z. Kristallogr. Cryst. Mater.* **2017**, *232 (12)*, 843–849. DOI: https://doi.org/10.1515/zkri-2017-2114

[15] K. F. Kalz, R. Kraehnert, M. Dvoyashkin, R. Dittmeyer, R. Gläser, U. Krewer, K. Reuter, J.-D. Grunwaldt, *ChemCatChem* **2017**, *9 (1)*, 17–29. DOI: https://doi.org/10.1002/cctc.201600996

[16] A. Urakawa, A. Baiker, *Top. Catal.* **2009**, *52 (10)*, 1312–1322. DOI: https://doi.org/10.1007/s11244-009-9312-3

[17] J.-D. Grunwaldt, B. Kimmerle, A. Baiker, P. Boye, C. G. Schroer, P. Glatzel, C. N. Borca, F. Beckmann, *Catal. Today* **2009**, *145 (3)*, 267–278. DOI: https://doi.org/10.1016/j.cattod.2008.11.002

[18] I. L. C. Buurmans, B. M. Weckhuysen, *Nat. Chem.* **2012**, *4 (11)*, 873–886. DOI: https://doi.org/10.1038/nchem.1478

[19] F. Meirer, B. M. Weckhuysen, *Nat. Rev. Mater.* **2018**, *3 (9)*, 324–340. DOI: https://doi.org/10.1038/s41578-018-0044-5

[20] L. Mino, E. Borfecchia, J. Segura-Ruiz, C. Giannini, G. Martinez-Criado, C. Lamberti, *Rev. Mod. Phys.* **2018**, *90 (2)*, 025007. DOI: https://doi.org/10.1103/RevModPhys.90.025007

[21] C. Jacobsen, *X-Ray Microscopy*, Cambridge University Press, Cambridge **2019**.

[22] J.-D. Grunwaldt, C. G. Schroer, *Chem. Soc. Rev.* **2010**, *39 (12)*, 4741–4753. DOI: https://doi.org/10.1039/C0CS00036A

[23] A. M. Beale, S. D. M. Jacques, B. M. Weckhuysen, *Chem. Soc. Rev.* **2010**, *39 (12)*, 4656–4672. DOI: https://doi.org/10.1039/C0CS00089B

[24] S. Mitchell, N.-L. Michels, K. Kunze, J. Pérez-Ramírez, *Nat. Chem.* **2012**, *4 (10)*, 825–831. DOI: https://doi.org/10.1038/nchem.1403

[25] A. M. Beale, S. D. M. Jacques, E. K. Gibson, M. Di Michiel, *Coord. Chem. Rev.* **2014**, *277–278*, 208–223. DOI: https://doi.org/10.1016/j.ccr.2014.05.008

[26] S. Weber, R. T. Zimmermann, J. Bremer, K. L. Abel, D. Poppitz, N. Prinz, J. Ilsemann, S. Wendholt, Q. Yang, R. Pashminehazar, F. Monaco, P. Cloetens, X. Huang, C. Kübel, E. Kondratenko, M. Bauer, M. Bäumer, M. Zobel, R. Gläser, K. Sundmacher, T. L. Sheppard, *ChemCatChem* **2022**, *14 (8)*, e202101878. DOI: https://doi.org/10.1002/cctc.202101878

[27] M. Thommes, K. Kaneko, A. V. Neimark, J. P. Olivier, F. Rodriguez-Reinoso, J. Rouquerol, K. S. W. Sing, *Pure Appl. Chem.* **2015**, *87 (9–10)*, 1051–1069. DOI: https://doi.org/10.1515/pac-2014-1117

[28] F. Tariq, P. D. Lee, R. Haswell, D. W. McComb, *Chem. Eng. Sci.* **2011**, *66 (23)*, 5804–5812. DOI: https://doi.org/10.1016/j.ces.2011.07.034

[29] F. Tariq, R. Haswell, P. D. Lee, D. W. McComb, *Acta Mater.* **2011**, *59 (5)*, 2109–2120. DOI: https://doi.org/10.1016/j.actamat.2010.12.012

[30] J. Becher, T. L. Sheppard, S. Fam, S. Baier, W. Wang, D. Wang, S. Kulkarni, T. F. Keller, M. Lyubomirskiy, D. Brueckner, M. Kahnt, A. Schropp, C. G. Schroer, J.-D. Grunwaldt, *J. Phys. Chem. C* **2019**, *123 (41)*, 25197–25208. DOI: https://doi.org/10.1021/acs.jpcc.9b06541

[31] Y. Fam, T. L. Sheppard, A. Diaz, T. Scherer, M. Holler, W. Wang, D. Wang, P. Brenner, A. Wittstock, J.-D. Grunwaldt, *ChemCatChem* **2018**, *10 (13)*, 2858–2867. DOI: https://doi.org/10.1002/cctc.201800230

[32] S. Weber, K. L. Abel, R. T. Zimmermann, X. Huang, J. Bremer, L. K. Rihko-Struckmann, D. Batey, S. Cipiccia, J. Titus, D. Poppitz, C. Kübel, K. Sundmacher, R. Gläser, T. L. Sheppard, *Catalysts* **2020**, *10 (12)*, 1471. DOI: https://doi.org/10.3390/catal10121471

[33] B. Apeleo Zubiri, J. Wirth, D. Drobek, S. Englisch, T. Przybilla, T. Weissenberger, W. Schwieger, E. Spiecker, *Adv. Mater. Interfaces* **2021**, *8 (4)*, 2001154. DOI: https://doi.org/10.1002/admi.202001154

[34] T. Weissenberger, R. Leonhardt, B. A. Zubiri, M. Pitínová-Štekrová, T. L. Sheppard, B. Reiprich, J. Bauer, R. Dotzel, M. Kahnt, A. Schropp, C. G. Schroer, J.-D. Grunwaldt, J. L. Casci, J. Čejka, E. Spiecker, W. Schwieger, *Chem. – Eur. J.* **2019**, *25 (63)*, 14430–14440. DOI: https://doi.org/10.1002/chem.201903287

[35] M. Holler, A. Diaz, M. Guizar-Sicairos, P. Karvinen, E. Färm, E. Härkönen, M. Ritala, A. Menzel, J. Raabe, O. Bunk, *Sci. Rep.* **2014**, *4 (1)*, 3857. DOI: https://doi.org/10.1038/srep03857

[36] H. Mimura, S. Handa, T. Kimura, H. Yumoto, D. Yamakawa, H. Yokoyama, S. Matsuyama, K. Inagaki, K. Yamamura, Y. Sano, K. Tamasaku, Y. Nishino, M. Yabashi, T. Ishikawa, K. Yamauchi, *Nat. Phys.* **2010**, *6 (2)*, 122–125. DOI: https://doi.org/10.1038/nphys1457

[37] R. Caulkin, X. Jia, C. Xu, M. Fairweather, R. A. Williams, H. Stitt, M. Nijemeisland, S. Aferka, M. Crine, A. Léonard, D. Toye, P. Marchot, *Ind. Eng. Chem. Res.* **2009**, *48 (1)*, 202–213. DOI: https://doi.org/10.1021/ie800033a

[38] J. von Seckendorff, K. Achterhold, F. Pfeiffer, R. Fischer, O. Hinrichsen, *Powder Technol.* **2021**, *380*, 613–628. DOI: https://doi.org/10.1016/j.powtec.2020.11.026

[39] X. Ou, X. Zhang, T. Lowe, R. Blanc, M. N. Rad, Y. Wang, N. Batail, C. Pham, N. Shokri, A. A. Garforth, P. J. Withers, X. Fan, *Mater. Charact.* **2017**, *123*, 20–28. DOI: https://doi.org/10.1016/j.matchar.2016.11.013

[40] P. Kočí, M. Isoz, M. Plachá, A. Arvajová, M. Václavík, M. Svoboda, E. Price, V. Novák, D. Thompsett, *Catal. Today* **2019**, *320*, 165–174. DOI: https://doi.org/10.1016/j.cattod.2017.12.025

[41] E. Bianchi, T. Heidig, C. G. Visconti, G. Groppi, H. Freund, E. Tronconi, *Catal. Today* **2013**, *216*, 121–134. DOI: https://doi.org/10.1016/j.cattod.2013.06.019

[42] E. Bianchi, G. Groppi, W. Schwieger, E. Tronconi, H. Freund, *Chem. Eng. J.* **2015**, *264*, 268–279. DOI: https://doi.org/10.1016/j.cej.2014.11.055

[43] C. Sinn, G. R. Pesch, J. Thöming, L. Kiewidt, *Int. J. Heat Mass Transfer* **2019**, *139*, 600–612. DOI: https://doi.org/10.1016/j.ijheatmasstransfer.2019.05.042

[44] M. Sadeghi, M. Mirdrikvand, G. R. Pesch, W. Dreher, J. Thöming, *Exp. Fluids* **2020**, *61 (5)*, 124. DOI: https://doi.org/10.1007/s00348-020-02960-4

[45] W. C. Conner, S. W. Webb, P. Spanne, K. W. Jones, *Macromolecules* **1990**, *23 (2)*, 4742–4747. DOI: https://doi.org/10.1021/ma00224a002

[46] M. A. Ferrero, R. Sommer, P. Spanne, K. W. Jones, W. C. Conner, *J. Polym. Sci., Part A: Polym. Chem.* **1993**, *31 (10)*, 2507–2512. DOI: https://doi.org/10.1002/pola.1993.080311011

[47] G. Hofmann, A. Rochet, E. Ogel, M. Casapu, S. Ritter, M. Ogurreck, J.-D. Grunwaldt, *RSC Adv.* **2015**, *5 (9)*, 6893–6905. DOI: https://doi.org/10.1039/C4RA14007A

[48] W. Kaltner, K. Lorenz, B. Schillinger, A. Jentys, J. A. Lercher, *Catal. Lett.* **2010**, *134 (1)*, 24–30. DOI: https://doi.org/10.1007/s10562-009-0221-7

[49] E. K. Gibson, M. W. Zandbergen, S. D. M. Jacques, C. Biao, R. J. Cernik, M. G. O'Brien, M. Di Michiel, B. M. Weckhuysen, A. M. Beale, *ACS Catal.* **2013**, *3 (3)*, 339–347. DOI: https://doi.org/10.1021/cs300746a

[50] H. Silva, M. G. Nielsen, E. M. Fiordaliso, C. D. Damsgaard, C. Gundlach, T. Kasama, I. B. Chorkendorff, D. Chakraborty, *Appl. Catal., A* **2015**, *505*, 548–556. DOI: https://doi.org/10.1016/j.apcata.2015.07.016

[51] F. Pfeiffer, *Nat. Photonics* **2018**, *12 (1)*, 9–17. DOI: https://doi.org/10.1038/s41566-017-0072-5

[52] P. Cloetens, W. Ludwig, J. Baruchel, D. Van Dyck, J. Van Landuyt, J. P. Guigay, M. Schlenker, *Appl. Phys. Lett.* **1999**, *75 (19)*, 2912–2914. DOI: https://doi.org/10.1063/1.125225

[53] J. C. da Silva, K. Mader, M. Holler, D. Haberthür, A. Diaz, M. Guizar-Sicairos, W.-C. Cheng, Y. Shu, J. Raabe, A. Menzel, J. A. van Bokhoven, *ChemCatChem* **2015**, *7 (3)*, 413–416. DOI: https://doi.org/10.1002/cctc.201402925

[54] S. Weber, A. Diaz, M. Holler, A. Schropp, M. Lyubomirskiy, K. L. Abel, M. Kahnt, A. Jeromin, S. Kulkarni, T. F. Keller, R. Gläser, T. L. Sheppard, *Adv. Sci.* **2022**, *9 (8)*, 2105432. DOI: https://doi.org/10.1002/advs.202105432

[55] S. Weber, D. Batey, S. Cipiccia, M. Stehle, K. L. Abel, R. Gläser, T. L. Sheppard, *Angew. Chem., Int. Ed.* **2021**, *60 (40)*, 21772–21777. DOI: https://doi.org/10.1002/anie.202106380

[56] M. Veselý, R. Valadian, L. M. Lohse, M. Toepperwien, K. Spiers, J. Garrevoet, E. T. C. Vogt, T. Salditt, B. M. Weckhuysen, F. Meirer, *ChemCatChem* **2021**, *13 (10)*, 2494–2507. DOI: https://doi.org/10.1002/cctc.202100276

[57] J. Ihli, R. R. Jacob, M. Holler, M. Guizar-Sicairos, A. Diaz, J. C. da Silva, D. Ferreira Sanchez, F. Krumeich, D. Grolimund, M. Taddei, W. C. Cheng, Y. Shu, A. Menzel, J. A. van Bokhoven, *Nat. Commun.* **2017**, *8 (1)*, 809. DOI: https://doi.org/10.1038/s41467-017-00789-w

[58] J. Ihli, A. Diaz, Y. Shu, M. Guizar-Sicairos, M. Holler, K. Wakonig, M. Odstrcil, T. Li, F. Krumeich, E. Müller, W.-C. Cheng, J. Anton van Bokhoven, A. Menzel, *J. Phys. Chem. C* **2018**, *122 (40)*, 22920–22929. DOI: https://doi.org/10.1021/acs.jpcc.8b05624

[59] H. Friedrich, P. E. de Jongh, A. J. Verkleij, K. P. de Jong, *Chem. Rev.* **2009**, *109 (5)*, 1613–1629. DOI: https://doi.org/10.1021/cr800434t

[60] J. Zečević, K. P. de Jong, P. E. de Jongh, *Curr. Opin. Solid State Mater. Sci.* **2013**, *17 (3)*, 115–125. DOI: https://doi.org/10.1016/j.cossms.2013.04.002

[61] J. M. Thomas, C. Ducati, R. Leary, P. A. Midgley, *ChemCatChem* **2013**, *5 (9)*, 2560–2579. DOI: https://doi.org/10.1002/cctc.201200883

[62] J. Wirth, S. Englisch, D. Drobek, B. Apeleo Zubiri, M. Wu, N. Taccardi, N. Raman, P. Wasserscheid, E. Spiecker, *Catalysts* **2021**, *11 (7)*, 810. DOI: https://doi.org/10.3390/catal11070810

[63] O. Daoura, G. Fornasieri, M. Boutros, N. El Hassan, P. Beaunier, C. Thomas, M. Selmane, A. Miche, C. Sassoye, O. Ersen, W. Baaziz, P. Massiani, A. Bleuzen, F. Launay, *Appl. Catal., B* **2021**, *280*, 119417. DOI: https://doi.org/10.1016/j.apcatb.2020.119417

[64] G. Prieto, J. Zečević, H. Friedrich, K. P. de Jong, P. E. de Jongh, *Nat. Mater.* **2013**, *12 (1)*, 34–39. DOI: https://doi.org/10.1038/nmat3471

[65] M. Blažek, M. Žalud, P. Kočí, A. York, C. M. Schlepütz, M. Stampanoni, V. Novák, *Chem. Eng. J.* **2021**, *409*, 128057. DOI: https://doi.org/10.1016/j.cej.2020.128057

[66] K. W. Bossers, R. Valadian, S. Zanoni, R. Smeets, N. Friederichs, J. Garrevoet, F. Meirer, B. M. Weckhuysen, *J. Am. Chem. Soc.* **2020**, *142 (8)*, 3691–3695. DOI: https://doi.org/10.1021/jacs.9b13485

[67] K. W. Bossers, R. Valadian, J. Garrevoet, S. van Malderen, R. Chan, N. Friederichs, J. Severn, A. Wilbers, S. Zanoni, M. K. Jongkind, B. M. Weckhuysen, F. Meirer, *JACS Au* **2021**, *1 (6)*, 852–864. DOI: https://doi.org/10.1021/jacsau.1c00130

[68] M. J. Werny, R. Valadian, L. M. Lohse, A.-L. Robisch, S. Zanoni, C. Hendriksen, B. M. Weckhuysen, F. Meirer, *Chem. Catal.* **2021**, *1 (7)*, 1413–1426. DOI: https://doi.org/10.1016/j.checat.2021.10.008

[69] E. T. C. Vogt, B. M. Weckhuysen, *Chem. Soc. Rev.* **2015**, *44 (20)*, 7342–7370. DOI: https://doi.org/10.1039/C5CS00376H

[70] F. Meirer, S. Kalirai, D. Morris, D. Soparawalla, Y. Liu, G. Mesu, C. Andrews Joy, M. Weckhuysen Bert, *Sci. Adv.* **2015**, *1 (3)*, e1400199. DOI: https://doi.org/10.1126/sciadv.1400199

[71] H. S. Cerqueira, G. Caeiro, L. Costa, F. Ramôa Ribeiro, *J. Mol. Catal.* **2008**, *292 (1)*, 1–13. DOI: https://doi.org/10.1016/j.molcata.2008.06.014

[72] J. Ruiz-Martínez, A. M. Beale, U. Deka, M. G. O'Brien, P. D. Quinn, J. F. W. Mosselmans, B. M. Weckhuysen, *Angew. Chem., Int. Ed.* **2013**, *52 (23)*, 5983–5987. DOI: https://doi.org/10.1002/anie.201210030

[73] S. R. Bare, M. E. Charochak, S. D. Kelly, B. Lai, J. Wang, Y.-c. K. Chen-Wiegart, *ChemCatChem* **2014**, *6 (5)*, 1427–1437. DOI: https://doi.org/10.1002/cctc.201300974

[74] S. Kalirai, U. Boesenberg, G. Falkenberg, F. Meirer, B. M. Weckhuysen, *ChemCatChem* **2015**, *7 (22)*, 3674–3682. DOI: https://doi.org/10.1002/cctc.201500710

[75] F. Meirer, D. T. Morris, S. Kalirai, Y. Liu, J. C. Andrews, B. M. Weckhuysen, *J. Am. Chem. Soc.* **2015**, *137 (1)*, 102–105. DOI: https://doi.org/10.1021/ja511503d

[76] M. Gambino, M. Veselý, M. Filez, R. Oord, D. Ferreira Sanchez, D. Grolimund, N. Nesterenko, D. Minoux, M. Maquet, F. Meirer, B. M. Weckhuysen, *Angew. Chem., Int. Ed.* **2020**, *59 (10)*, 3922–3927. DOI: https://doi.org/10.1002/anie.201914950

[77] J. Ihli, D. Ferreira Sanchez, R. R. Jacob, V. Cuartero, O. Mathon, F. Krumeich, C. Borca, T. Huthwelker, W.-C. Cheng, Y. Shu, S. Pascarelli, D. Grolimund, A. Menzel, J. A. van Bokhoven, *Angew. Chem., Int. Ed.* **2017**, *56 (45)*, 14031–14035. DOI: https://doi.org/10.1002/anie.201707154

[78] B. M. Weckhuysen, *Chem. Commun.* **2002**, *2*, 97–110. DOI: https://doi.org/10.1039/B107686H

[79] A. Chakrabarti, M. E. Ford, D. Gregory, R. Hu, C. J. Keturakis, S. Lwin, Y. Tang, Z. Yang, M. Zhu, M. A. Bañares, I. E. Wachs, *Catal. Today* **2017**, *283*, 27–53. DOI: https://doi.org/10.1016/j.cattod.2016.12.012

[80] A. I. Frenkel, J. A. Rodriguez, J. G. Chen, *ACS Catal.* **2012**, *2 (11)*, 2269–2280. DOI: https://doi.org/10.1021/cs3004006

[81] J. Becher, D. F. Sanchez, D. E. Doronkin, D. Zengel, D. M. Meira, S. Pascarelli, J.-D. Grunwaldt, T. L. Sheppard, *Nat. Catal.* **2021**, *4 (1)*, 46–53. DOI: https://doi.org/10.1038/s41929-020-00552-3

[82] S. W. T. Price, D. J. Martin, A. D. Parsons, W. A. Sławiński, A. Vamvakeros, S. J. Keylock, A. M. Beale, J. F. W. Mosselmans, *Sci. Adv.* **2017**, *3 (3)*, e1602838. DOI: https://doi.org/10.1126/sciadv.1602838

[83] K. H. Cats, J. C. Andrews, O. Stéphan, K. March, C. Karunakaran, F. Meirer, F. M. F. de Groot, B. M. Weckhuysen, *Catal. Sci. Technol.* **2016**, *6 (12)*, 4438–4449. DOI: https://doi.org/10.1039/C5CY01524C

[84] A. Vamvakeros, S. D. M. Jacques, M. Di Michiel, D. Matras, V. Middelkoop, I. Z. Ismagilov, E. V. Matus, V. V. Kuznetsov, J. Drnec, P. Senecal, A. M. Beale, *Nat. Commun.* **2018**, *9 (1)*, 4751. DOI: https://doi.org/10.1038/s41467-018-07046-8

[85] B. M. Weckhuysen, *Phys. Chem. Chem. Phys.* **2003**, *5 (20)*, 4351–4360. DOI: https://doi.org/10.1039/B309650P

[86] F. C. Meunier, *Chem. Soc. Rev.* **2010**, *39 (12)*, 4602–4614. DOI: https://doi.org/10.1039/B919705M

[87] N. E. Tsakoumis, A. P. E. York, D. Chen, M. Rønning, *Catal. Sci. Technol.* **2015**, *5 (11)*, 4859–4883. DOI: https://doi.org/10.1039/C5CY00269A

[88] M. A. Newton, S. Checchia, A. J. Knorpp, D. Stoian, W. van Beek, H. Emerich, A. Longo, J. A. van Bokhoven, *Catal. Sci. Technol.* **2019**, *9 (12)*, 3081–3089. DOI: https://doi.org/10.1039/C9CY00464E

[89] I. D. Gonzalez-Jimenez, K. Cats, T. Davidian, M. Ruitenbeek, F. Meirer, Y. Liu, J. Nelson, J. C. Andrews, P. Pianetta, F. M. F. de Groot, B. M. Weckhuysen, *Angew. Chem., Int. Ed.* **2012**, *51 (48)*, 11986–11990. DOI: https://doi.org/10.1002/anie.201204930

[90] K. H. Cats, I. D. Gonzalez-Jimenez, Y. Liu, J. Nelson, D. van Campen, F. Meirer, A. M. J. van der Eerden, F. M. F. de Groot, J. C. Andrews, B. M. Weckhuysen, *Chem. Commun.* **2013**, *49 (41)*, 4622–4624. DOI: https://doi.org/10.1039/C3CC00160A

[91] A. Vamvakeros, S. D. M. Jacques, V. Middelkoop, M. Di Michiel, C. K. Egan, I. Z. Ismagilov, G. B. M. Vaughan, F. Gallucci, M. van Sint Annaland, P. R. Shearing, R. J. Cernik, A. M. Beale, *Chem. Commun.* **2015**, *51 (64)*, 12752–12755. DOI: https://doi.org/10.1039/C5CC03208C

[92] A. S. Fjellvåg, P. S. Jørgensen, D. Waller, D. S. Wragg, M. D. Michiel, A. O. Sjåstad, *Materialia* **2022**, *21*, 101359. DOI: https://doi.org/10.1016/j.mtla.2022.101359

[93] D. Matras, A. Vamvakeros, S. D. M. Jacques, M. di Michiel, V. Middelkoop, I. Z. Ismagilov, E. V. Matus, V. V. Kuznetsov, R. J. Cernik, A. M. Beale, *J. Mater. Chem. A* **2021**, *9 (18)*, 11331–11346. DOI: https://doi.org/10.1039/D1TA01464A

[94] D. Matras, A. Vamvakeros, S. D. M. Jacques, V. Middelkoop, G. Vaughan, M. Agote Aran, R. J. Cernik, A. M. Beale, *Phys. Chem. Chem. Phys.* **2020**, *22 (34)*, 18964–18975. DOI: https://doi.org/10.1039/D0CP02144J

[95] D. Matras, S. D. M. Jacques, H. R. Godini, M. Khadivi, J. Drnec, A. Poulain, R. J. Cernik, A. M. Beale, *J. Phys. Chem. C* **2018**, *122 (4)*, 2221–2230. DOI: https://doi.org/10.1021/acs.jpcc.7b11573

[96] A. Vamvakeros, D. Matras, S. D. M. Jacques, M. di Michiel, S. W. T. Price, P. Senecal, M. A. Aran, V. Middelkoop, G. B. G. Stenning, J. F. W. Mosselmans, I. Z. Ismagilov, A. M. Beale, *J. Catal.* **2020**, *386*, 39–52. DOI: https://doi.org/10.1016/j.jcat.2020.03.027

[97] P. Senecal, S. D. M. Jacques, M. Di Michiel, S. A. J. Kimber, A. Vamvakeros, Y. Odarchenko, I. Lezcano-Gonzalez, J. Paterson, E. Ferguson, A. M. Beale, *ACS Catal.* **2017**, *7 (4)*, 2284–2293. DOI: https://doi.org/10.1021/acscatal.6b03145

[98] J. Becher, S. Weber, D. Ferreira Sanchez, D. E. Doronkin, J. Garrevoet, G. Falkenberg, D. Motta Meira, S. Pascarelli, J.-D. Grunwaldt, T. L. Sheppard, *Catalysts* **2021**, *11 (4)*, 459. DOI: https://doi.org/10.3390/catal11040459

[99] A. G. Greenaway, I. Lezcano-Gonzalez, M. Agote-Aran, E. K. Gibson, Y. Odarchenko, A. M. Beale, *Top. Catal.* **2018**, *61 (3)*, 175–182. DOI: https://doi.org/10.1007/s11244-018-0888-3

[100] A. H. Clark, R. J. G. Nuguid, P. Steiger, A. Marberger, A. W. Petrov, D. Ferri, M. Nachtegaal, O. Kröcher, *ChemCatChem* **2020**, *12 (5)*, 1429–1435. DOI: https://doi.org/10.1002/cctc.201901916

[101] K. A. Lomachenko, E. Borfecchia, C. Negri, G. Berlier, C. Lamberti, P. Beato, H. Falsig, S. Bordiga, *J. Am. Chem. Soc.* **2016**, *138 (37)*, 12025–12028. DOI: https://doi.org/10.1021/jacs.6b06809

[102] C. G. Schroer, I. Agapov, W. Brefeld, R. Brinkmann, Y.-C. Chae, H.-C. Chao, M. Eriksson, J. Keil, X. Nuel Gavalda, R. Rohlsber-ger, O. H. Seeck, M. Sprung, M. Tischer, R. Wanzenberg, E. Weckert, *J. Synchrotron Radiat.* **2018**, *25 (5)*, 1277–1290. DOI: https://doi.org/10.1107/S1600577518008858

[103] E. Maire, C. Le Bourlot, J. Adrien, A. Mortensen, R. Mokso, *Int. J. Fract.* **2016**, *200 (1)*, 3–12. DOI: https://doi.org/10.1007/s10704-016-0077-y

[104] N. Martensson, M. Eriksson, *Nucl. Instrum. Methods Phys. Res., Sect. A* **2018**, *907*, 97–104. DOI: https://doi.org/10.1016/j.nima.2018.03.018

[105] P. Raimondi, *Synchrotron Radiat. News* **2016**, *29 (6)*, 8–15. DOI: https://doi.org/10.1080/08940886.2016.1244462

New Dimensions in Catalysis Research with Hard X-Ray Tomography

Srashtasrita Das, Reihaneh Pashminehazar, Shweta Sharma, Sebastian Weber, Thomas L. Sheppard*

Review Article: Hard X-ray tomography offers a powerful and flexible toolkit for catalyst characterization: from spatially resolved studies at micro- to nanoscale; chemical contrast with X-ray absorption, fluorescence, diffraction, etc.; along with in situ/operando methods. This review highlights the bright future of hard X-ray tomography in catalysis. .... ◼

10 cm

1 cm

1 mm

www.cit-journal.com